1   **Assessment of LNAPL in Subsurface under Fluctuating Groundwater**

2   **Table using 2D Sand Tank Experiments**

3

4   Pankaj Kumar Gupta[1], Basant Yadav[2], Brijesh Kumar Yadav[3]

5

6   [1]Research Scholar, Indian Institute of Technology Roorkee

7   Postal Address: Department of Hydrology, IIT Roorkee-247667, Uttarakhand (India)

8   Email ID: pgupta@hy.iitr.ac.in

9

10   [2]Post-Doctoral Fellow, Rural Water Supply, Cranfield University, UK

11   Email ID: Basant.Yadav@cranfield.ac.uk

12

13   [3]Associate Professor, Indian Institute of Technology Roorkee

14   Postal Address: Department of Hydrology, IIT Roorkee-247667, Uttarakhand (India).

15   Email ID: brijkfhy@iitr.ac.in/ brijeshy@gmail.com

16

17   **Abstract**

18

19   The focus of this study was to investigate fate and transport of toluene, a light non-aqueous

20   phase liquids (LNAPL), in subsurface under dynamic groundwater table conditions. A series

21   of experiments were conducted using two-dimensional (2-D) sand tank setup having the

22   dimension of 125cm L×90cm H×10cm W and integrated with an auxiliary column of inner

23   diameter 14 cm and height 120 cm. In the beginning a steady state flow and LNAPL transport

24   experiment was conducted under stable groundwater table condition. Thereafter, three

25   groundwater table fluctuation experiments were conducted by rising and falling

26   groundwater table in 2, 4 and 8 hours to maintain a rapid, general, and slow fluctuation

27   conditions respectively. Pure phase of toluene was injected at the rate of 1mL/minute for

28   a total duration of 5 minutes. The soil-water and soil vapor samples were periodically

29   collected and analyzed for toluene concentrations. Later, the representation of 2-D sand

30   tank setup was numerically simulated to get the response of flow and the LNAPL transport

31   under varying groundwater table conditions. The analysis of the results show that a large

32   LNAPL pool area (250 cm^2) gets developed under rapid fluctuating groundwater condition

33   which significantly enhances the dissolution rate and contributes for a high concentration of

34   dissolved LNAPL to the receiving receptors. The mass transfer coefficient value of 9.50E-02;

35   5.80E-03; 3.50E-03; 1.20E-04 m/s was estimated for rapid, general, slow and stable

36   groundwater table conditions, respectively. Furthermore, the estimated Sherwood numbers (

37   Sh) were found 0.95, 16.20, 16.95 and 19.30 while Peclet numbers (P_e) were 1.80, 75.47,

38   80.14, and 95.06 for rapid, general, slow and stable cases respectively. This shows that the

39   dissolution is highly affected by groundwater table which may cause loss of pollutant mass as

40   a dissolved phase. However, the transport of dissolved LNAPL plume is comparatively fast in

41   case of rapid fluctuating groundwater, resulting in closely space concentration isolines of

42   toluene containing plume. A high biodegradation rate is observed in plume regions having

43   concentration ranges from 140-160 ppm, while it decreases in the plume regions having high

44   concentrations (>160 ppm) and low concentrations (<140ppm) in these cases. In sand tank,

45   the microbial growth was found to be increasing as plume moves away from the LNAPL pool

46   towards low-gradient, which fortifies detrimental impact of toluene on survival of indigenous

47   microorganisms near the LNAPL pool. The results of this study may help in implementing

48   effective remediation technique to decontaminate LNAPL polluted sites under fluctuating

49   groundwater table conditions, especially in (semi)-arid coastal aquifers.

50

53

54   **1. Introduction**

55   The subsurface contamination by LNAPL is widespread and challenging environmental

56   problem, especially in coastal regions having dynamic groundwater table condition due to tidal

57   effects. Most of the petroleum industries and refineries are located in coastal regions. The

58   leakage of LNAPL from subsurface storage tanks and disposal sites of effluents (Nema and

59   Gupta, 1999; Kumar et al. 2016) on surface are major source of hydrocarbons pollution of the

60   receiving environment, especially under varying subsurface conditions. When LNAPL is

61   released into (sub)-surface, it starts moving downward through the partially saturated zone, in

62   response to gravitational force, until it reaches to the capillary fringe (Das and Mirzaei, 2012;

63   Power et al. 1992a, b; 1994a, b; Illangasekare et al. 1995). A fraction of LNAPL mass is being

64   retained in partially saturated zone and LNAPL-air mass partition (i.e. volatilization process)

65   contributes as vapor phase contamination (Nambi and Powers, 2000; Brusseau et al. 2002,

66   Nambi and Powers, 2003, Patterson and Davis, 2009). The remaining pool of LNAPL provides

67 sufficient dissolving area to the underlying groundwater in smear zone which starts dissolving

68 with flowing groundwater and create a dissolved phase plume (Lee and Chrysikopoulos, 1998;

69 Kim and Chrysikopoulos, 1999; Nema and Gupta, 2003; Oostrom et al. 2006; 2007). Molecular

70 diffusion and mechanical dispersion along with advective flux cause spreading of dissolved

71 plume to downgradient receiving locations (Das, 2002; Yadav and Hassanizadeh, 2011; Picone

72 et al. 2013). On the other hand, native potential microbes play significant role to degrade the

73 dissolved LNAPL from polluted zone (Yadav et al. 2013; Basu et al. 2015, Mustapha et al.

74 2018).

75   Groundwater flow regimes play a significant role in the dissolution of pure phase

76 LNAPL pool and its movement to the surrounding locations (Das and Nassehi, 2003; Dobson

77 et al. 2007; Sulaymon and Gzar, 2011, Kamaruddin et al. 2011; Yadav et al. 2012). Dynamic

78 nature of groundwater table causes significant spreading of pooled LNAPL in smear zone,

79 which considerably increases the LNAPL-water interphase area and resulted in accelerated

80 dissolution (Mobile et al. 2012; Vasudevan et al. 2014). Variations in groundwater table not

81 only causes changes in the soil-water system, but also impacts the LNAPL pool behavior, if it

82 is present on the water table and in the underlying saturated zone. The LNAPL lying on the top

83 of the groundwater table moves down with it when the water table lowers and leave a trail of

84 LNAPL in the unsaturated zone in the form of isolated ganglia. Subsequently when the

85 groundwater table rises, the LNAPL pool also moves upward leaving behind a trapped amount

86 of LNAPL in the form of disconnected blobs in the saturated zone (Lenhard et al. 2004;

87 Kechavarzi et al. 2005). A part of the residual LNAPL in unsaturated zone gets mobilized again

88 when the groundwater table rises. Thus, a dynamic groundwater table accelerates the

89 dissolution of pure phase LNAPL resulting in high concentration of LNAPL plume (Legout et

90 al. 2009). The dissolved LNAPL plume then moves along with groundwater and forms a

91 polluted zone which features with varying concentration levels (Neale et al. 2000; Rolle et al.

92 2009; Zhang et al. 2014; Zhou et al. 2015; Sarikurt et al. 2017).

93   There is a paucity of knowledge on the impact of dynamic groundwater table conditions

94 on LNAPL behaviors in subsurface. Groundwater fluctuation is significantly affected by heavy

95 pumping rates to irrigate agricultural land and concurrent recharge due to return flow. Typically

96 for shallow aquifers, a high pumping rates and return flow/recharge may cause rapid fluctuation

97 of groundwater table. While, a slow pumping and less return flow/recharge may lead to

98 general/slow groundwater table fluctuation. Different nature of rainfall events is also

99 responsible for such a rapid and slow fluctuation of groundwater table. Fluctuations in the

100 groundwater table due to various reasons including tidal effects have a profound influence on

101   the spatial distribution, dissolution and biodegradation of LNAPL in the subsurface
102   environment. This phenomenon is predominantly observed in shallow aquifer regions where
103   most of the petrochemical industries and refineries are located and potentially at high risk of
104   LNAPL release from the subsurface storage tanks. Thus, an extensive study was conducted to
105   investigate LNAPL fate and transport under fluctuating groundwater table conditions using a
106   series of 2-D sand tank experiments. A better understanding of fate and transport of LNAPL
107   under varying subsurface water table condition is required which in turn can help in designing
108   effectively remediation technologies and to accurately predict their clean-up times and the
109   associated cost.

110

111   **2. Materials and Methods**

112   In this study, the behavior of pooled pure phase LNAPL and its dissolved plume in subsurface
113   under stable and fluctuating groundwater table conditions is investigated using a series of two-
114   dimensional laboratory experiments and numerical modelling. The preliminary experiments
115   were conducted to characterize the flow and transport parameters of the developed
116   subsurface soil-water system. Mechanical sieve analysis was performed to find the
117   particle size distribution of the sand which is listed in Table 1 along with other physical
118   parameters. The porosity of sand packing was determined using oven dry and volumetric
119   methods. Further, the hydraulic conductivity of the system was estimated using a constant
120   head permeameter. To see the behavior of the pooled LNAPL and dissolved phase plume, a
121   series of two dimensional sand tank experiments were performed by considering varying
122   groundwater table conditions. A two dimensional sand tank setup filled with homogenous sand
123   was used to conduct the laboratory experiment under (1) steady-state groundwater condition
124   and (2) three different dynamic groundwater table fluctuation conditions, separately. Lastly,
125   the soil-water system was numerically simulated using HYDRUS 2D model considering the
126   laboratory investigated soil-water and solute transport parameters.

127

128

129

130

131

132

133

134

135   Table 1. Properties of the sand used in the laboratory experiments.

Characteristic	Values
Type	Medium Sand
Grain Size	0.5-1 mm
Particle Size > 1 mm	1.71±0.5%
Particle Size 0.5mm-1mm	98.27±0.5%
Particle Size < 0.5 mm	0.02±0.01%
Effective Porosity	0.33±0.02%
Bulk Density	1.52 ±0.1g/cm^3
Grain Density	2.31±0.1 g/cm^3

136

2.1 Two Dimensional Sand Tank Setup

137

138   Two dimensional sand tank setup used in the study was specially designed using 2.5 mm thick
139   stainless steel formed box with inner dimensions of 150 cm-long × 120 cm-high ×10 cm-deep
140   (Figure 1). Two wells were installed at each side of tank and front cover of the tank was made-
141   up of a thick glass sheet for enabling observations. Indian standard clean sand (650 grade-II)
142   of particle size 0.5-1mm free from organic matter was packed in the central chamber between
143   both the wells up to a height of 90 cm. The top 30 cm thick sand pack was kept as head-space
144   to maintain aerobic condition. The porous media was oversaturated before pouring it into the
145   column setup to create a homogenous packing. During this filling, a comb-like metallic tool
146   was used to smooth the sand surface for avoiding a layered structure of the porous media. The
147   extra water was then gravitationally drained out from the bottom of tank setup. The system was
148   then flushed at maximum velocity until the effluent water was free of suspended fine material.
149   After each of the experiments, the used sand was replaced with fresh sand pack the new set of
150   the experiments following the packing procedure as describes earlier. The wells were used as
151   upstream (high pressure) and downstream (low pressure) reservoir to maintain the water table.
152   An auxiliary column containing the collected groundwater was connected to the inlet port of
153   upstream well with viton tubes of a peristaltic pump. This peristaltic pump refers as "upstream
154   pump" was used to supply the groundwater to the sand tank through the upstream well. The
155   objective of this auxiliary column was to provide sufficient groundwater storage required to
156   maintain the dynamic groundwater table conditions (Figure 1a). Similarly, the outlet of the

157 downstream well was connected to another peristaltic pump (refer herein as downstream pump)

158 to extract the groundwater and recirculate to the auxiliary column. The flow rate of the pumps

159 was adjustable so that the desired pressure difference in the two reservoirs can be maintained

160 and thereby controlling the groundwater flow within the tank setup. A LNAPL release port was

161 installed just below the top surface of sand packing about 20 cm from the upstream well. The

162 sampling ports having equal horizontal spacing of 15.5 cm are situated at 30 and 60 cm height

163 from the bottom of the tank setup in two horizontal layers (figure 1b). Piezometers were

164 attached to the tank to measure the positions of the groundwater table during experiments.

165 Filtration screens were fixed around the inlet and outlet valves to prevent the entrance of the

166 sand particles in the connecting viton tubes.

167 A series of tracer transport experiments were performed to determine the longitudinal

168 and vertical dispersivity of sand under fast, base and slow groundwater velocities. A solution

169 of tap water and sodium chloride with an initial concentration of 1000 mg/l was continuously

170 injected to the tank for the selected groundwater fluctuation cases. The water samples were

171 routinely collected from the sampling port located at 50 cm away (at X:45; Y:50 cm) in the

172 lower-gradient side from the injection port of the top sampling layer and the tracer

173 concentrations were measured using portable conductivity meter. The longitudinal dispersivity

174 (D_L) resulted from the dispersivity flux were estimated using the breakthrough curves (BTCs)

175 obtained from the tracer experiments. Time values corresponding to relative concentration

176 ratios of 84%, 50%, and 16% were used in calculating the dispersion coefficient (D_L) and

177 longitudinal dispersivity (α_L) as proposed by Sulaymon and Gzar (2011). In the equation,

178 $D_{ij} = \tau D_* + D_x$, the first term resulted from diffusive flux was estimated by multiplying the

179 diffusion coefficient of toluene i.e. 6.3×10^{-6} [cm^2/sec] and tortuosity of sand i.e. 1.43

180 (Sulaymon and Gzar, 2011). The vertical dispersivity (D_V) were considered 0.1 times of the

181 obtained longitudinal dispersivity (Dobson et al. 2007).

182 A series of LNAPL transport experiments were performed using 2D sand tank setup for

183 stable/steady and three different groundwater table level conditions. Under steady-state

184 condition, a constant groundwater flux was applied as inflow (using the upstream pump) and

185 the same was extracted as outflow (using the down-stream pump) to maintain a constant flow

186 velocity in the horizontal direction and, hence, keeping the water table location at a constant

187 height. However, in rapid, general and slow groundwater level fluctuation experiments the

188 inflow/outflow flux were controlled by peristaltic pump to maintain a raising of the water

189 table by 5cm in 1, 2, and 4 hours respectively. The groundwater table was then lowered

190 in the same manner; a drop of 5 cm was achieved in subsequent 1, 2 and 4 hours for rapid,

191 general and slow fluctuation conditions, respectively. It may be noted herein that "one

192 fluctuation cycle" refers to a complete high-low-high cycle of groundwater table levels.

193

194
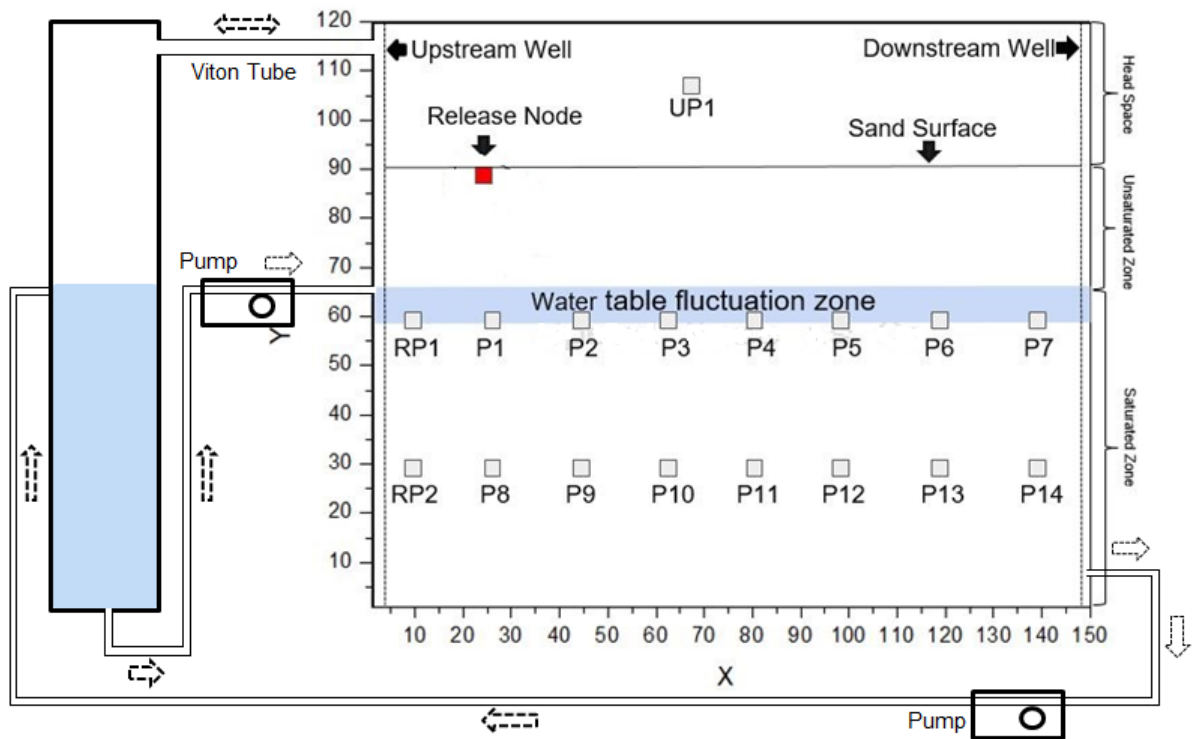
196 Figure 1. Schematic diagram of 2D sand tank setup integrated with an auxiliary column

197 used to investigate fate and transport of LNAPL in subsurface under dynamic

198 groundwater table conditions.

199

200 Rising of groundwater table was maintained by pumping the water from the

201 auxiliary column to the upstream well and closing the outflow from the downstream well

202 for a target duration of respective fluctuation conditions. Likewise, groundwater falling

203 was maintained by extracting water from the downstream well and closing the inflow to

204 the sand tank from the auxiliary column for the same duration. Such switching of the

205 peristaltic pump was adjustable and calibrated for a target duration of respective

206 fluctuation conditions. A brief pumping details of different considered cases are listed in

207 Table 2. To maintain a rise and fall of 5 cm, (150 cm-long $\times$ 05 cm-magnitude of fluctuation

208 $\times$ 10 cm-deep $\times$ 33% porosity) 0.002475 m^3 or 2.475 liters of groundwater was required as

209 inflow and outflow. Pure phase toluene was released from the top surface of the tank set up

210 to create a pool of the LNAPL above the groundwater table which was varied in the range of
211 55-60 cm level from the tank bottom. The toluene (Merck with 99.9 % purity) was injected
212 at a constant rate of 02 ml/min for a duration of 5 minutes using an air-tight syringe.
213 Periodically, a small amount of soil water samples from both the layers and the soil vapor
214 samples from head-space were collected carefully for the analysis.
215
216 Table 2. Inflow and outflow pumping strategies of groundwater table fluctuation cases.

Conditions	Inflow Pumping		Outflow pumping		Total Duration	Pumping Rate
	Rise	Fall	Rise	Fall		
Rapid fluctuation	1 hour	✕	✕	1 hour	2 hours	2475.0 mL/hr
General fluctuation	2 hours	✕	✕	2 hours	4 hours	1237.5 mL/hr
Slow fluctuation	4 hours	✕	✕	4 hours	8 hours	618.7 mL/hr

217
218
219 **2.2 Sample Analysis**
220 Soil water samples were collected periodically using needles attached with syringes
221 (Hamilton gold) from the sampling ports embedded in the sampling layers in saturated zone
222 (Figure 1). The samples were transferred into vials (Agilent vials: Agilent Product No.
223 5190/1599) having air tight red septa caps without any air contacts. Similarly, soil vapor
224 samples were collected from sampling ports installed in the headspace. The collected
225 samples were analyzed using Gas chromatography-mass spectrometry (GC-MS) (Agilent
226 7890B) in triplicates. A chrompack capillary column (30m×0.25mm, Silicone coating of
227 0.25µm) was used for toluene analysis. Helium was employed as the carrier gas at a flow rate
228 of 25 mL/min. Similarly, air and nitrogen were used with a flow rate of 20 mL/min during GC-
229 MS analysis. During the measurements, temperature of injection port, oven, and detector port
230 was kept at 150°C, 120°C, and 150°C, respectively. One set of collected samples were also
231 analyzed using gas chromatography/combustion/isotope ratio mass spectrometry
232 (GC/C/IRMS) technique to capture pure phase LNAPL (Dempster et al. 1997).
233
234

2.3 Microbiological Analysis

The microbial population in the soil water zone was counted using heterotrophic or standard plate count methods (No. 9215C). In this method, colony forming units (CFU) for live heterotrophic bacteria was estimated from the collected soil-water samples during laboratory experiments. The soil water samples for microbial population count were collected from M1 and M7 ports of top layer and M8 and M14 ports of bottom layer (Fig 2). After the sample collection, all the collected samples were diluted with a factor of 10^1 to 10^{-5} and mechanically shaken for 15 seconds. Growth media was prepared using a combination of 20g protease peptone; 1.5g of K_2HPO_4; 1.5 g of $MgSO_4.7H_2O$; and 20g of Agar. Final pH of media was adjusted to 7.2 by adding $1N$ NaOH, before autoclaving at 121^0C for 15 minutes. The laminar air flow setup was wiped with the 70% ethanol and UV light for the 15 minutes to avoid any background microbial contaminations. Well marked (sample number, dilution, and date) plates were poured with 30mL prepared growth media and kept still for few minutes to solidify agar surface. Thereafter, diluted samples were inoculated with the help of spreader on agar surface of respective plates. Successively, all the plates were incubated for 48 hours at 36±1°C for. After the incubation, colony was counted manually using the quadrate method. Plates having an un-countable number (or too numerous) was considered as overgrowth. In this study, microbial populations were counted with the 12 hours' interval to see the impact of LNAPL transport on microbial growth under fluctuating groundwater table conditions. Thus, above mentioned microbial counting procedures were performed for each experiments separately. A comparative account of such bacterial count during groundwater table fluctuation experiments gives a clear idea on how groundwater fluctuating conditions affects the LNAPL fate and transport in the subsurface.

3. Numerical Modeling

To solve the dissolved phase LNAPL transport in saturated zone 2D form of mass balance equation used as:

$$\frac{\partial}{\partial t}(nS_f C_{if}) = -\nabla.(q_f C_{if}) + \nabla.(nS_f D_{if}.\nabla C_{if}) + K_{if} - S \tag{1}$$

Where C_{if} is NAPL compound in f phase [ML^{-3}], q_f is discharge through soil profile [LT^{-1}], n is porosity of soil [L^{3}L^{-3}], t is time [T], K_{if} is the dissolution rate of LNAPL [ML^{-3}T^{-1}] was observed using characteristic length of LNAPL pool and equilibrium concentration in dissolved

267   phase. Likewise, S is biodegradation rate [$ML^{-3}T^{-1}$] (as sink term) was obtained using (control

268   and live) microcosms experiments. D_{if} is hydrodynamic dispersion [L^2T^{-1}] which was obtained

269   using breakthrough curves (BTCs) of tracer transport experiment. The HYDRUS 2D model

270   was used to solve governing equation for water flow and solute transport (Simunek et al. 1996).

271   A two dimensional numerical domain having similar dimension of sand tank was created to

272   simulate soil water flow and LNAPL transport through saturated zones. Thus, in this case S_f

273   i.e. fluid saturation in pore space [L^3L^{-3}] was taken as 1 as the media fully saturated. The

274   simulation domain was discretised in small grids of size 1 mm in a hexahedral geometry for

275   solving the governing equation numerically. The Galerkin finite elements method integrated

276   with Crank-Nicholson iterative scheme was used for the solution. The soil water flow and

277   solute transport parameters listed in table 1 were used as model input parameters. The hydraulic

278   behavior or parameters were obtained by inverse solution in HYDRUS 2D (Simunek et al.,

279   2012).

280

281   **3.1 Initial and boundary conditions**

282   The simulation domain was assigned no background concentration (zero) as initial solute

283   condition. The saturated moisture content was taken as the initial moisture level of the domain

284   and the top boundary was considered as the water table. Right side boundary (was taken as

285   continuous flux by incorporating respective pulse of influx for 1, 2, and 4 hours to maintain

286   groundwater table fluctuation along with base groundwater velocity. Similarly, left side

287   boundary was taken as a pulse out-flux for the respective cases. In case of stable groundwater

288   table condition, constant influx and out-flux was taken without pulse condition. No flux

289   condition was considered as the lower boundary condition. A LNAPL releasing point was

290   incorporated at same location as of two dimensional laboratory sand tank setup.

291

292   **4. Results and Discussion**

293

294   The breakthrough curves (BTCs) of tracer experiments under stable and different groundwater

295   fluctuation cases are presented in Figure 2 for rapid, general and slow groundwater table

296   fluctuation conditions represented as GWTF-C1, GWTF-C2, GWTF-C3, respectively. The

297   slope of the BTCs shown in Figure 2 are of similar trend, suggesting that the sand was packed

298   uniformly in each set of experiments without any significant preferential flow paths. The best

299   fit values of dispersion coefficient values are 0.000246, 0.0000171, 0.0000108, 0.0000073

300   m^2/s for rapid, general, slow, and stable groundwater table fluctuation conditions respectively.

301   Similarly, estimated longitudinal dispersivity values are 1.23, 0.72, 0.28, 0.12m for rapid,

302   general, slow, and stable groundwater table fluctuation conditions respectively. The observed

303   values of dispersivity was used to simulate dissolved LNAPL plume in identified domain under
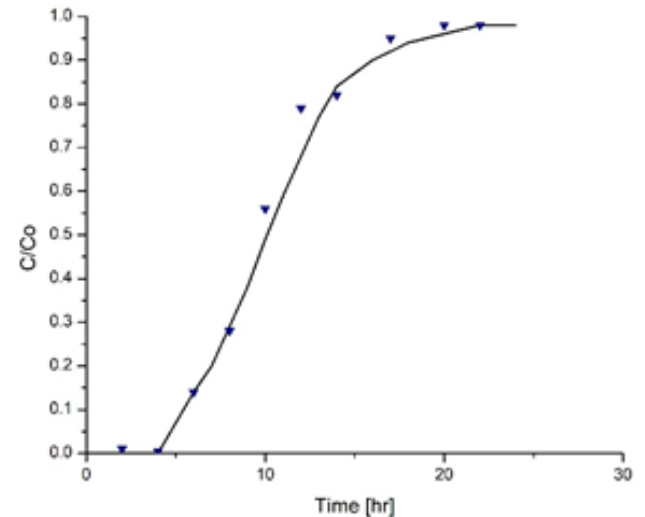
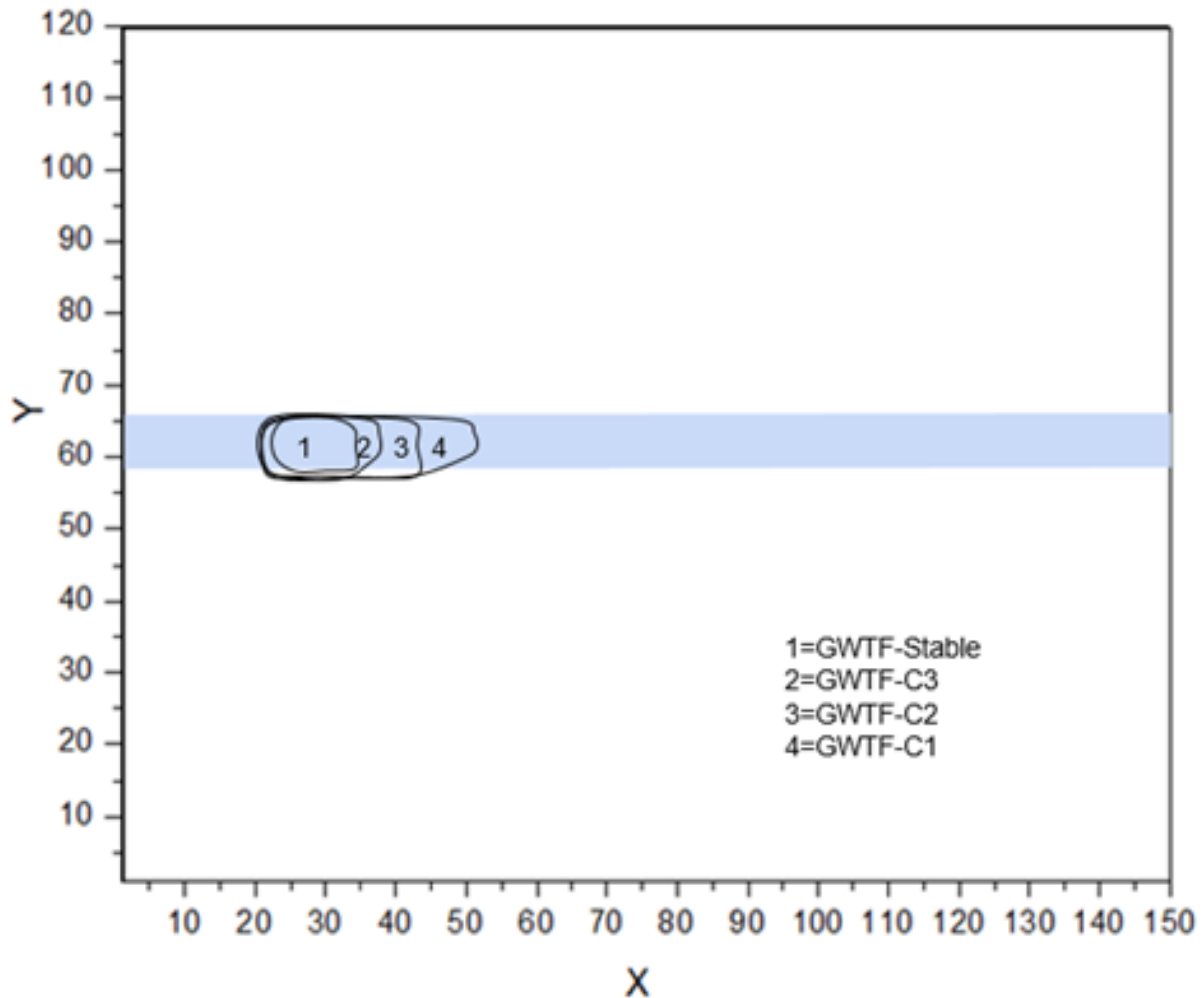304   corresponding groundwater table case.
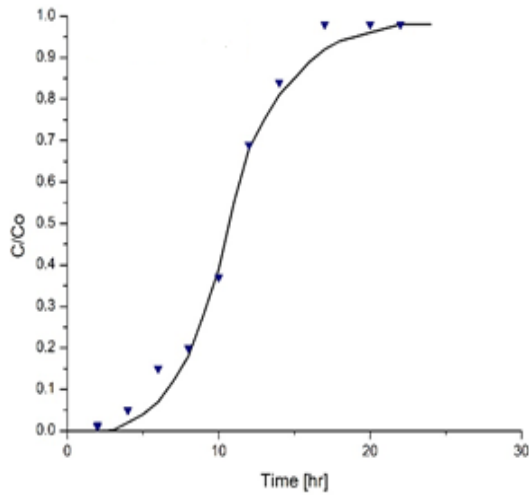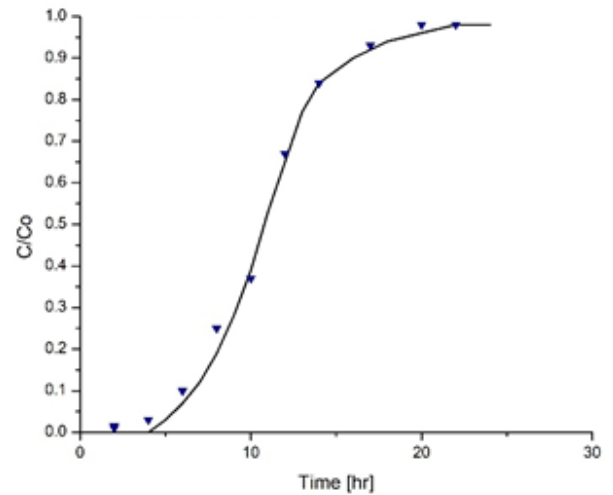
(a) GWTF-C1   **(b) GWTF-C2**
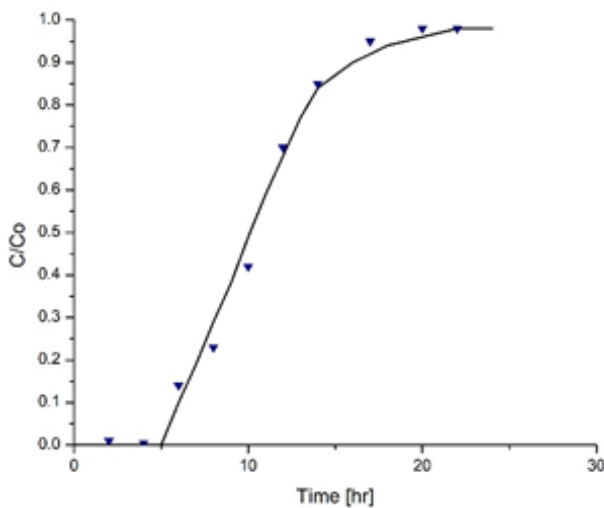
(c) GWTF-C3   **(d) GWTF-C4**

305

306

307   Figure 2: BTCs obtained from tracer test analysis for (a) rapid, (b) general, (c) slow and

308   (d) stable groundwater fluctuation conditions.

309

310

Figure 3: Coverage of the LNAPL pool in smear zone subjected to different groundwater fluctuation conditions.

4.1 Pure phase LNAPL coverage and dissolution

An effort has been made to capture LNAPL pool area in two dimensional sand tank experiments under stable and fluctuating groundwater cases. For this purpose, periodically soil-water samples were analyzed by GC-MS/IRMS technique (Dempster et al. 1997). The interpreted boundary of pure phase LNAPL pool is presented in Figure 3 which shows a total area of 250, 200, 160 and 70 cm^2 covered under rapid, general, slow and stable groundwater fluctuation cases, respectively.

Experimentally observed area of pure phase LNAPL pool was used to determine the characteristic length of the pool and for the estimation of dissolution rate. It can be observed from the results that the rapid groundwater fluctuation causes the pure phase LNAPL pool to spread over more area then the stable groundwater case. A high groundwater velocity

327   due to rapid fluctuation in groundwater governs the excess spreading of LNAPL in flow

328   directions. Spreading of pure phase LNAPL over a large area provides more dissolving surface

329   as LNAPL-water interphase to underlying flowing groundwater resulting into more dissolution

330   rates. Similarly, the large LNAPL pool contributes more LNAPL vapour to the overlying

331   unsaturated zone. Further, the volume of water contacting the LNAPL pool surface increases

332   as it spread in large area which also leads to high dissolution rates. This in turn significantly

333   increases dissolved phase concentration load to receiving groundwater and vapor

334   contamination to unsaturated pore air (Dobson et al. 2007; Vasudevan et al. 2014). On the other

335   hand, large coverage of pool contributes more LNAPL mass to capillary ganglia as smaller

336   blobs/fingering, which also play significant role in dissolution under rapid groundwater table

337   conditions. As noted by Sarikurt et al. (2017), the contact time and area of LNAPL-water

338   interphase is significant for dissolution rate and subsequent transport of dissolved LNAPL in

339   subsurface. Similarly, Sulaymon and Gzar (2011) highlighted that length of LNAPL-water

340   interphase plays important role to control the equilibrium concentration of dissolved LNAPL

341   plume. Results of this study confirm that the groundwater table fluctuation causes more

342   spreading of pure phase LNAPL pool itself which ultimately provide more LNAPL-water

343   dissolving area in smear zone. High dissolution rate from large LNAPL pool contributes high

344   concentration of dissolved LNAPL to the downgradient ports. The estimated LNAPL pool

345   coverage area under different cases can be used to forecast dissolved LNAPL plume under

346   dynamic groundwater flow conditions.

347

4.2 Vapor phase concentrations

349   The vapor phase LNAPL concentrations are plotted as BTC in Figure 4. The BTC shows a high

350   LNAPL concentration in case of rapid fluctuating groundwater table followed by general, slow

351   and stable groundwater table case. The vapor equilibrium concentration was observed as 210-

352   230 ppm in fluctuating condition while 180-185 ppm was observed in stable groundwater case.

353   This means a raising groundwater table carries pure phase LNAPL mass upward and a falling

354   groundwater allows LNAPL to move downward. During dynamics of groundwater level, the

355   trapped LNAPL remain behind in smear zone which creates a large interphase area of air-

356   LNAPL/water (Powers et al. 1992). Therefore, more vapor phase concentration was observed

357   from the residual LNAPL. These results are in line with the findings of study conducted by

358   Oostrom et al. (2006) with 2D experiments under water table dynamic conditions. The study

359   found a considerable residual LNAPL saturation in smear zone. The high vapor concentration

360   can also be attributed to the partition of LNAPL from large dissolved phase plume having high

concentration. Further, lowering of groundwater table increases air-filled porosity in smear zone, which eventually affects vapor phase LNAPL partition. The BTC of different groundwater table fluctuation experiments confirms that the vapor intrusion is highly dependent on the nature of groundwater table conditions (Patterson and Davis, 2009). High vapor LNAPL in unsaturated pores may become toxic for the indigenous microorganisms.
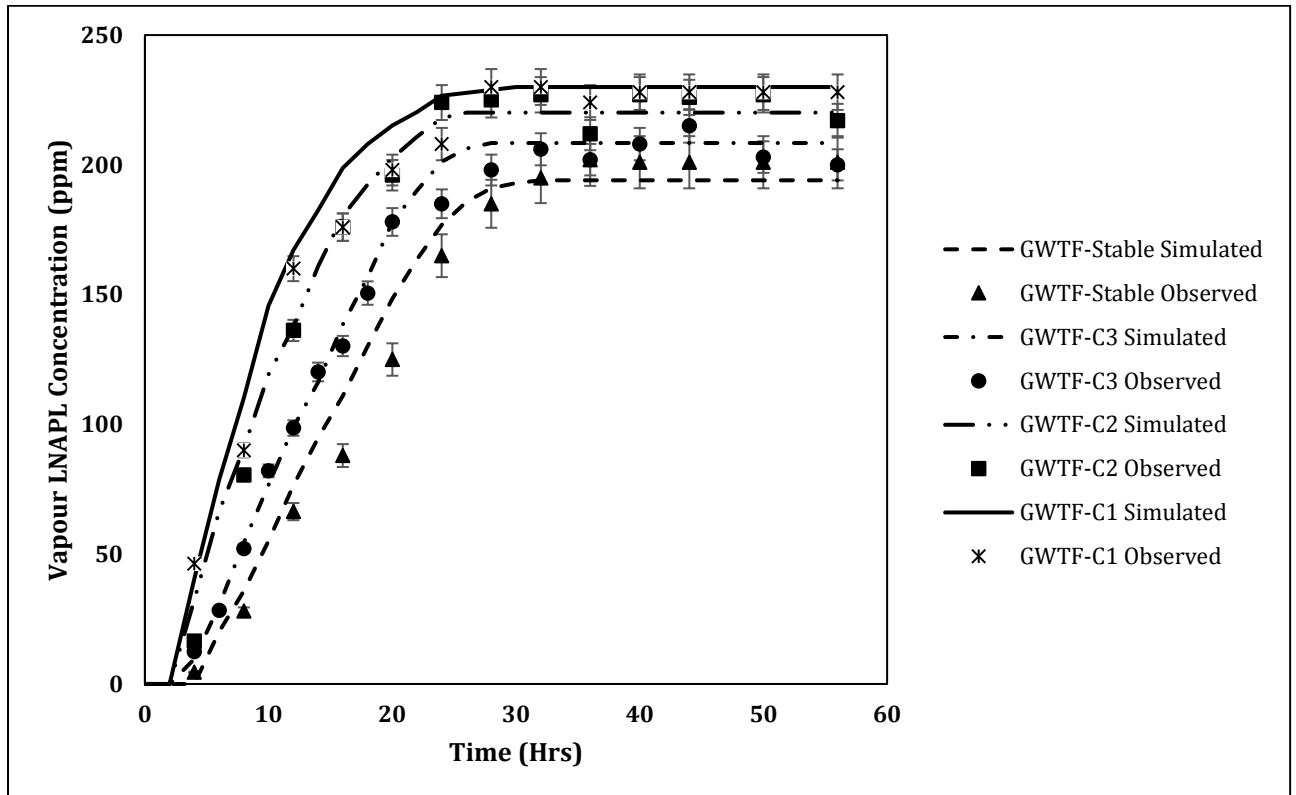

Figure 4: BTC representing LNAPL concentration in soil air in 2D sand tank under stable and fluctuation groundwater table conditions.

The measured pure phase LNAPL pool area was used to estimate its characteristic length of LNAPL pool ($l_{(c)}$) under stable and fluctuating groundwater conditions. The observed values of $l_{(c)}$ was found 15.81, 14.15, 12.64, and 8.36 cm under rapid, general, slow and stable groundwater fluctuation conditions, respectively. The estimated value of mass transfer coefficient (k^*) are listed in Table 3. The estimated Sherwood numbers (Sh) were found 0.95, 16.20, 16.95 and 19.30 while Peclet numbers (P_e) were 1.80, 75.47, 80.14, and 95.06 for rapid, general, slow and stable cases respectively. A high value of Sh indicates that dissolution was a dominating process under fluctuating groundwater conditions. The reason for high Sh can be

381   attributed to the large pool spreading, which provides more LNAPL-water interphase under

382   fluctuating groundwater condition. Further, more contact time of underlying groundwater with

383   the large dissolving LNAPL pool also accelerate the dissolution rate. Likewise, high P_e

384   indicates that the advective flow was dominant than the diffusive flow under fluctuating

385   groundwater conditions. However, one cannot ignore the importance of diffusive flux under

386   stable groundwater flow regimes. The correlation Sh with P_e is presented in Figure 5 with the

387   coefficient of determination (R^2) value of 0.998. This kind of high correlation between Sh and

388   P_e was also reported in a recent study by Sarikurt et al. (2017).

389

390
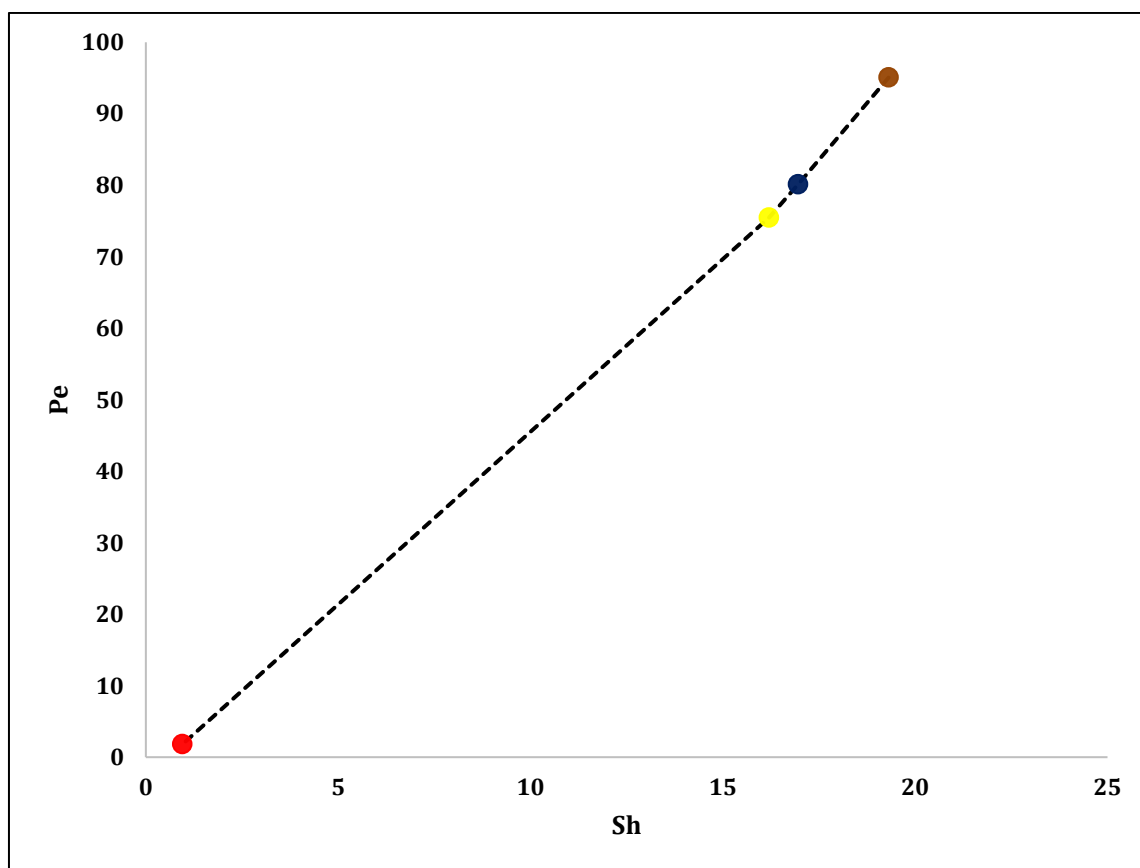
391

392   Figure 5: Correlation between Sh and P_e. Red, yellow, blue and green circle represent

393   stable, slow, general and rapid groundwater fluctuation conditions respectively.

394

395

396

397

Table 3: Estimated values of k^* and corresponding values of Sh and P_e under dynamic groundwater table conditions

Conditions	Mass transfer coefficient k^* (m/s)	Sherwood Number Sh (-)	Peclet Number P_e (-)
GWTF-C1	9.50E-02	19.30	95.06
GWTF-C2	5.80E-03	16.95	80.14
GWTF-C3	3.50E-03	16.20	75.47
GWTF-Stable	1.20E-04	0.95	1.80

4.3 Dissolved phase concentrations

Dissolved LNAPL concentrations as a function of time for all four cases are presented in figures 6-7. In figure 6a, BTC is presented for port 1 (top sampling layer: X:25cm; Y:60 cm) which was situated just below the water table and nearby LNAPL pool. It shows that toluene concentration starts rising after few hours and increases rapidly and then starts attenuating before reaching to a concentration of 200-230 ppm for rapid fluctuating groundwater case. Similar trends were observed for the remaining fluctuating groundwater cases. The higher concentration in the rapid fluctuation case was due to more dissolving LNAPL pool area than general, followed by slow and stable fluctuation conditions. Likewise, BTCs of port 4 and port 7 of upper layer are presented in figure 6b and 6c respectively. LNAPL concentration takes 10-12 hours and 20-26 hours to reach port 4 and port 7, which was 55 cm and 115 cm away from pool respectively. However, a significant difference in the final equilibrium concentration (plateau) was observed amongst different groundwater table fluctuation cases. At this stage the supply from the source and the out flux at the observed down-gradient port (port 7) was reaching to an equilibrium condition. A decreasing trend in the equilibrium concentration was observed as plume moves from up gradient location (port 1) to down-gradient locations (Port 4/7) which represents the dependency of biodegradation rate on dissolved LNAPL concentration. In general, the equilibrium concentration of toluene in earlier studies was found quite nearby to its dissolution limit. In this study, the observed concentration of toluene was not able to reach the maximum solubility value of toluene because of (a) limited contact (water-toluene) time of opportunity, (b) the concurrent biodegradation of the dissolved LNAPL in sand tank setup. The study shows that more than 150 ppm dissolved LNAPL concentration was found to start inhibiting metabolic actions of microbes causing lower degradation rates then its

424 potential rate. Similarly, a concentration less than 100 ppm provides insufficient carbon sources

425 to microbes resulting in comparatively low biodegradation rate of toluene. The optimal

426 biodegradation rate was found in plume area having concentrations ranges from 120-150 ppm,

427 especially under general groundwater condition. While biodegradation rate become quite slow

428 at port 1 due to high dissolved LNAPL concentration (>150 ppm) and causes toxicity to

429 potential microbes. The biodegradation rate in upper layer was accelerated by high diffusion

430 of oxygen from head space by fluctuating groundwater table.

431 Likewise, the dissolved LNAPL concentrations are presented in figures 7a-c for ports

432 8, 11 and 14 situated in bottom layer. Figure 7a shows that the dissolved LNAPL plume takes

433 10-12 hours to reach at port 8, which is at 30 cm downward from the pool. At port 8, there is

434 very less difference in equilibrium concentrations as compared to port 1. Whereas, a large

435 difference was found in equilibrium concentration of port 11 (Figure 7b) and port 14 (Figure

436 7c) in comparison to port 8 (Figure 7a). This seems due to high biodegradation rates at port 11

437 as compared to port 8, even the port 11 is situated in bottom layers where background oxygen

438 level is low.

439
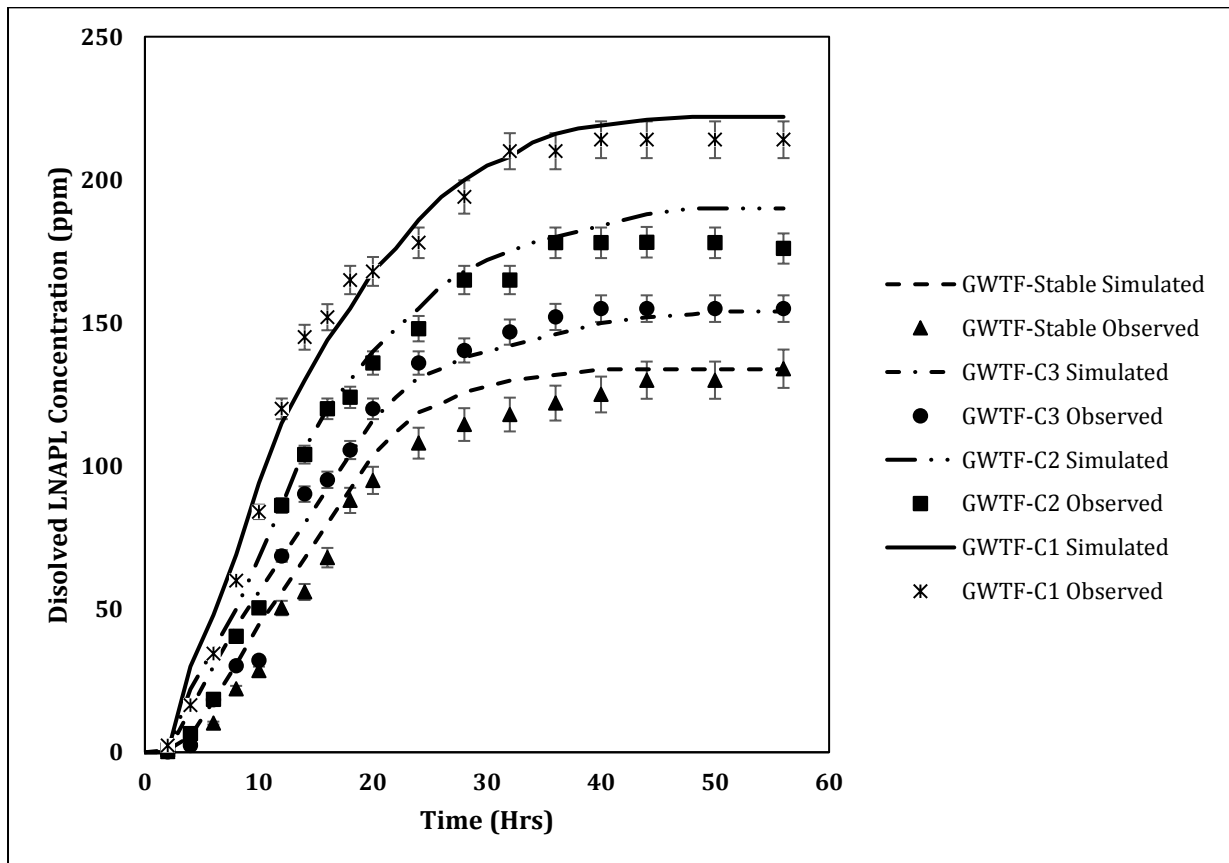
(a) Port 1: X:25; Y60
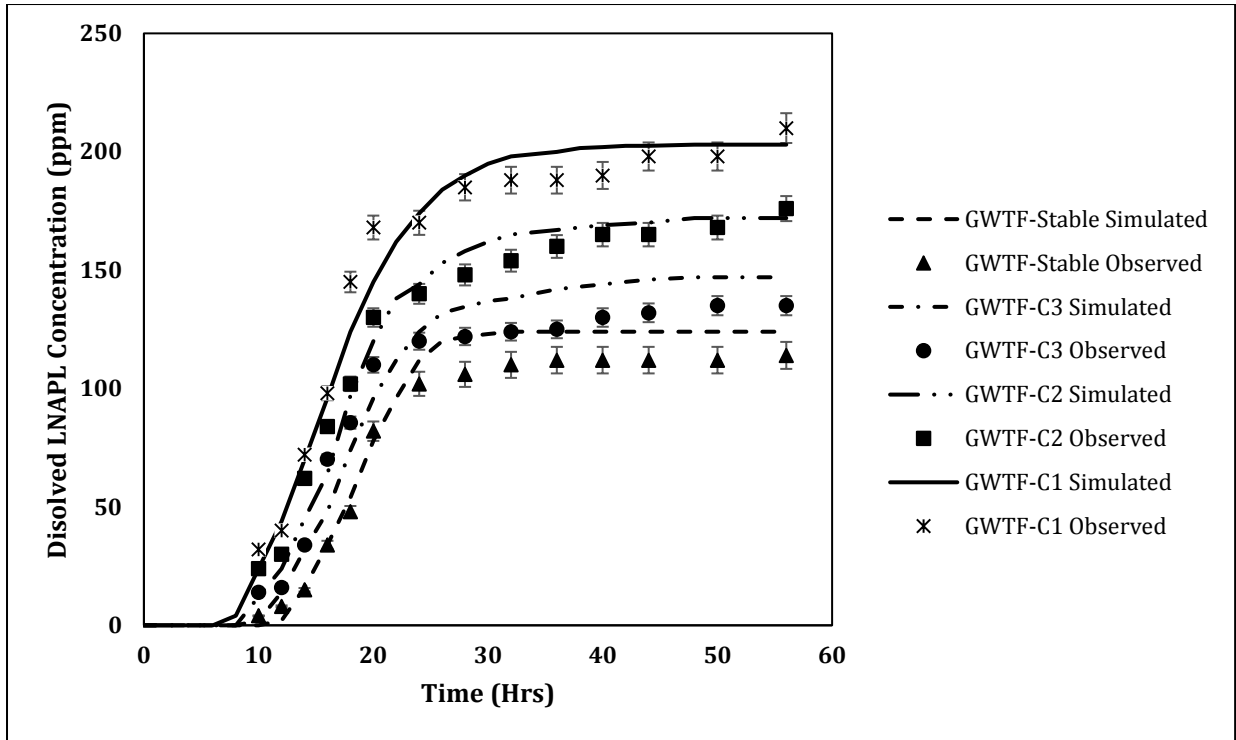
(b) Port 4: X:80; Y60
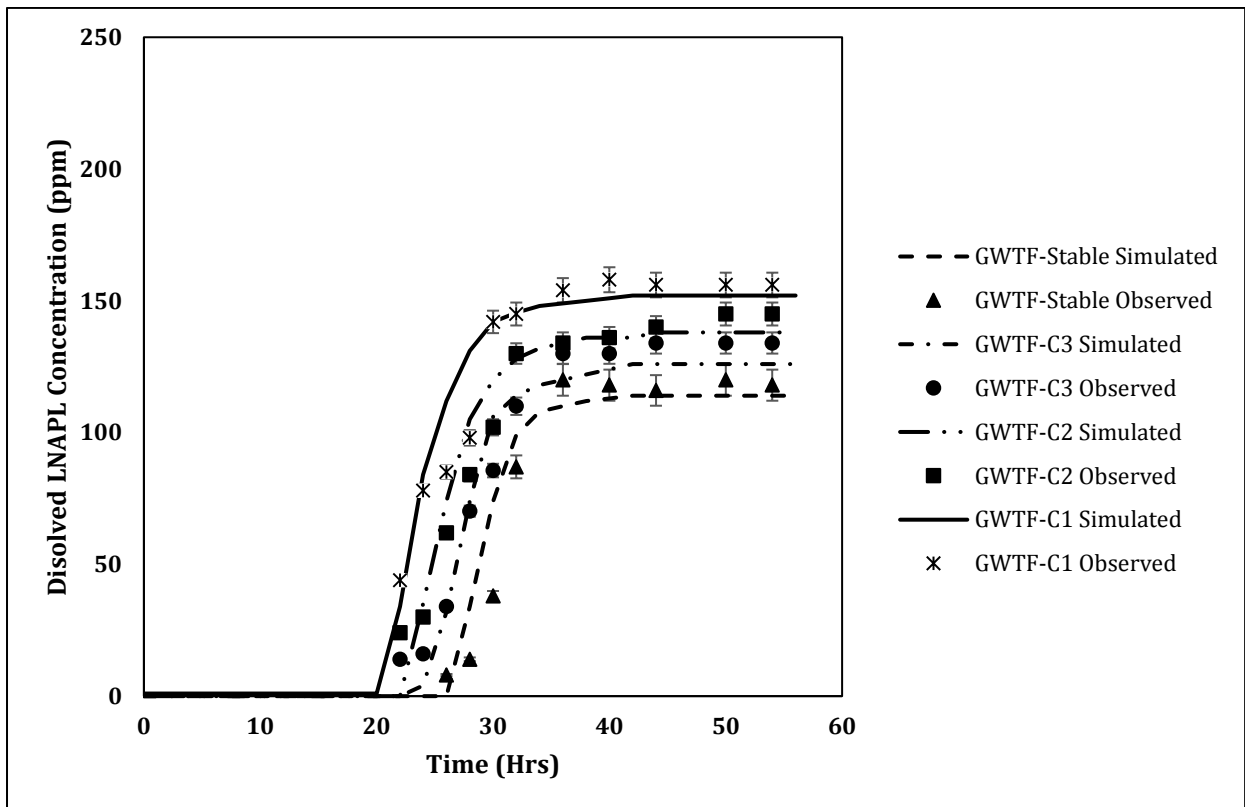
(c) Port 7: X:140; Y60

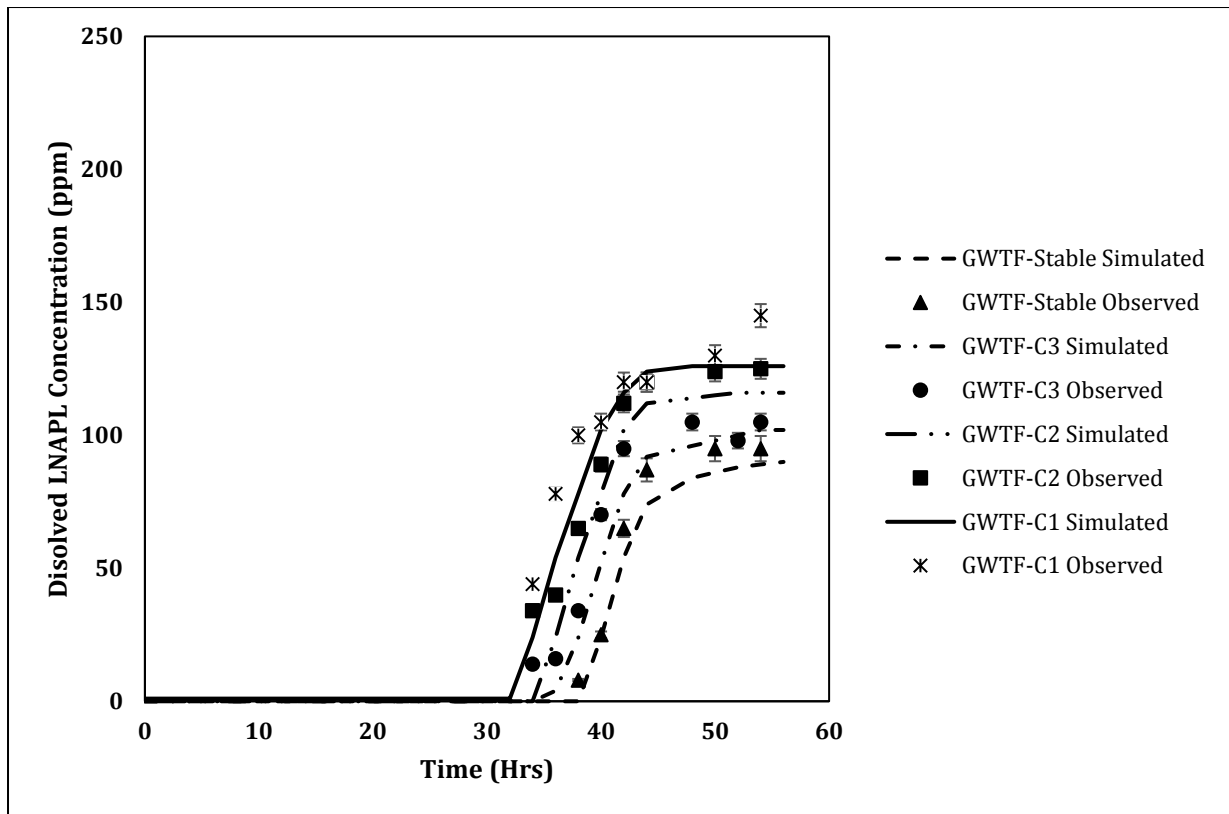Figure 6: BTCs of (a) port 1, (b) port 4 and (c) port 7 under stable and fluctuating groundwater table conditions.
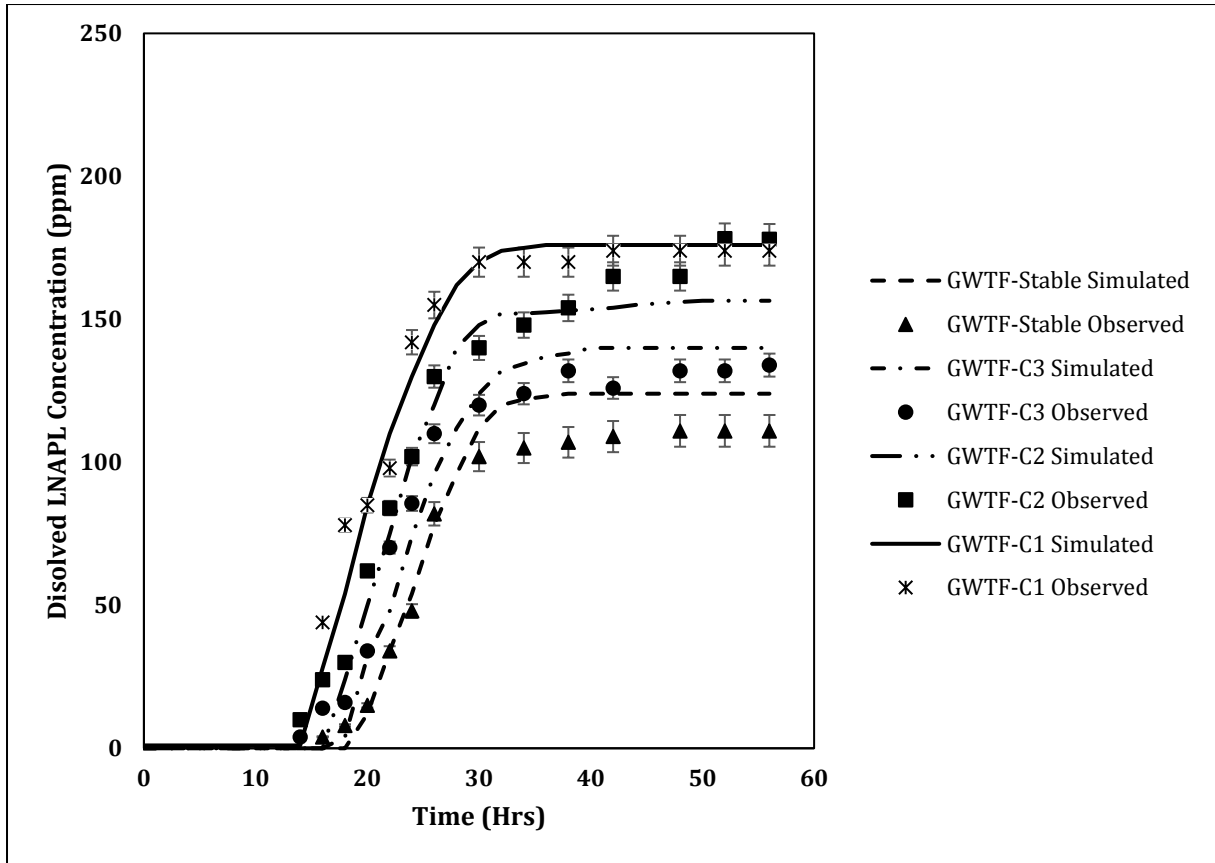
449
450   **(a) Port 8: X:25; Y30**

451
452   **(b) Port 11: X:80; Y30**

453
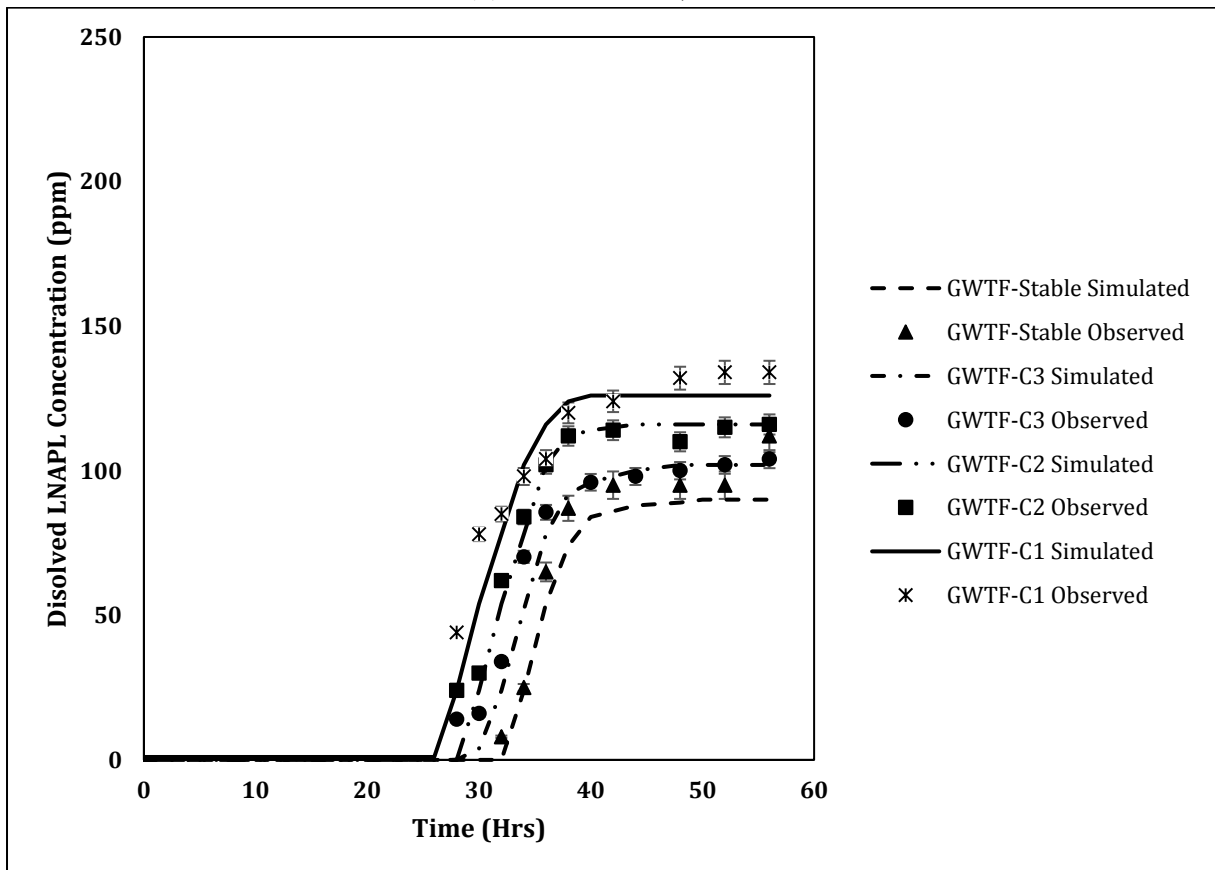
(c) Port 14: X:140; Y30

Figure 7: BTCs of (a) port 8, (b) port 11 and (c) port 14 under stable and fluctuating groundwater table conditions.

The experimentally observed dissolved LNAPL concentrations isolines are plotted as a function of space in figures 8a-d. These concentration isolines were plotted using experimentally measured data from all sampling ports (port1-14) including ports situated opposite to flow directions (port RP1-RP2). The objective of these isolines plot is to present different concentration zone originated from LNAPL pool under different selected groundwater table conditions. Figure 8a represents concentration isolines originated from large LNAPL pool having 15.81 cm under rapid groundwater table fluctuation condition. Thus, large dissolved plume was created with a concentration ranges from 120-160 ppm in initial 12 hours and later reaches up to 200 ppm nearby the pool location. A large area covered by high concentration i.e. greater than 150 ppm causes toxicity to potential microbes and thus low biodegradation rate was observed in this case. Thus, a closely spaced isolines were observed in rapid fluctuating groundwater conditions. Whereas, figure 8b represented isolines of dissolved plume originated from a pure phase LNAPL pool of characteristic length of 14.15 cm under general groundwater table fluctuation condition. In this case, the dissolved plume

474 concentration ranges 110 ppm-140 ppm in initial 12 hours and continuously increases upto 160

475 ppm. Less concentration (20ppm) of dissolved plume under general groundwater table

476 fluctuation condition was due to smaller LNAPL pool length then the rapid case. Thus, in

477 general groundwater table fluctuation case, a large area covered by 130-150ppm concentration

478 LNAPL plume become carbon source to potential microbes and causes enhanced

479 biodegradation rates. Similar trends were observed in case of slow groundwater table

480 fluctuation condition as presented in figure 8c. While, comparatively small dissolved LNAPL

481 plume (figure 8d) having less concentration (i.e. range of 70 ppm-100 ppm in initial 12 hours

482 and 80-120 ppm in 56 hours) was observed in case of stable groundwater case.

483   In this study, the concentration isolines clearly show the fast transport of dissolved

484 plume in horizontal direction than its transverse movement under stable and fluctuating

485 groundwater conditions. The horizontal spreading of plume was due to advection dominated

486 flow of the dissolved toluene originating from large contact area between LNAPL pool and

487 water. Dissolved LNAPL plume movement in opposite direction of groundwater flow driven

488 by diffusive flux is comparative very slow. Whereas, the expansion of dissolved LNAPL plume

489 in the vertical direction under fluctuating groundwater shows the crucial role of dispersive flux.

490 The diffusive flux of the dissolved LNAPL can play a crucial role in LNAPL movement under

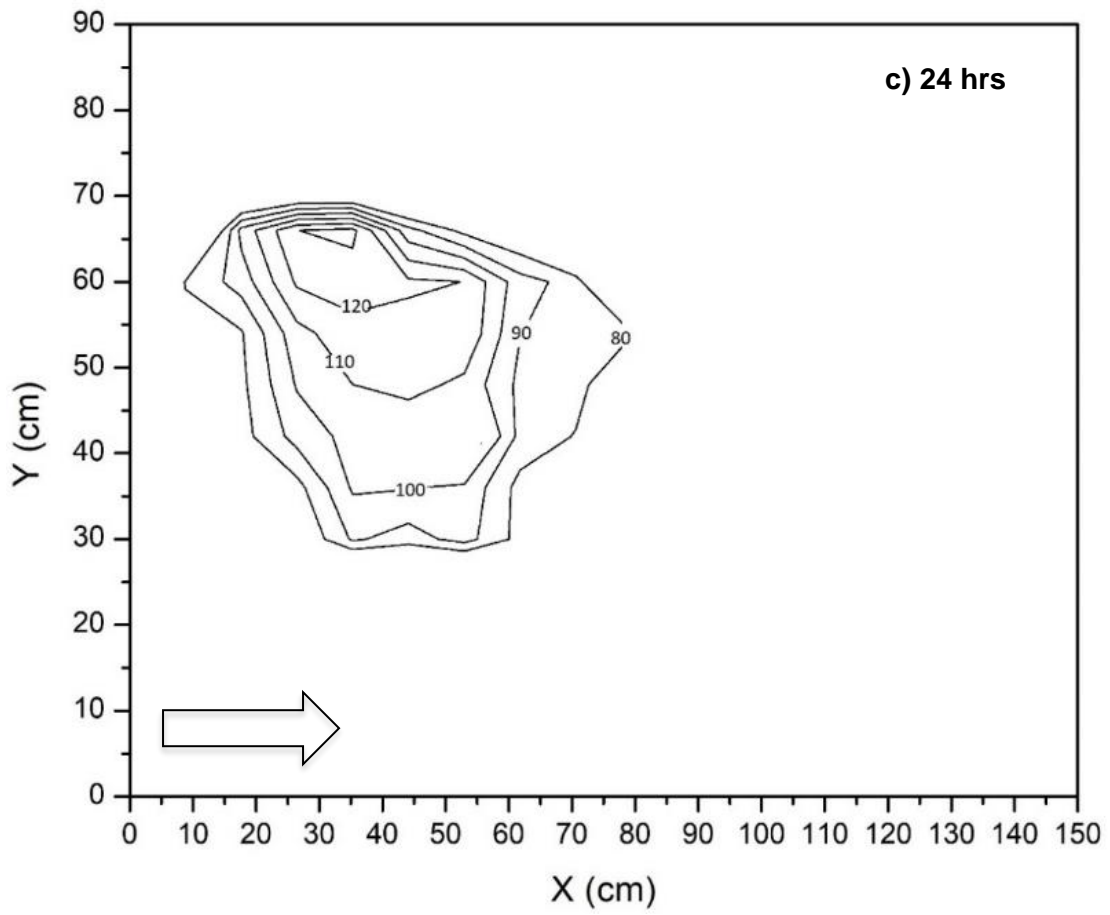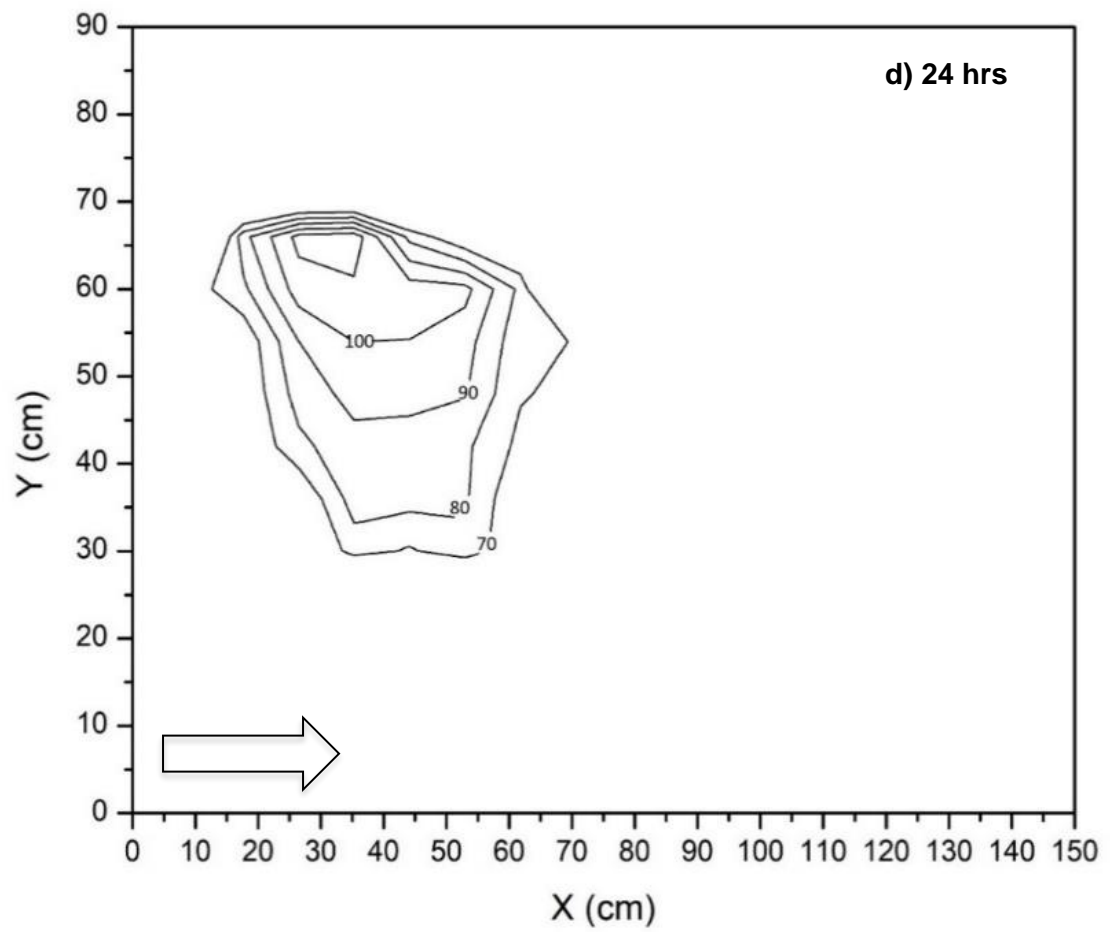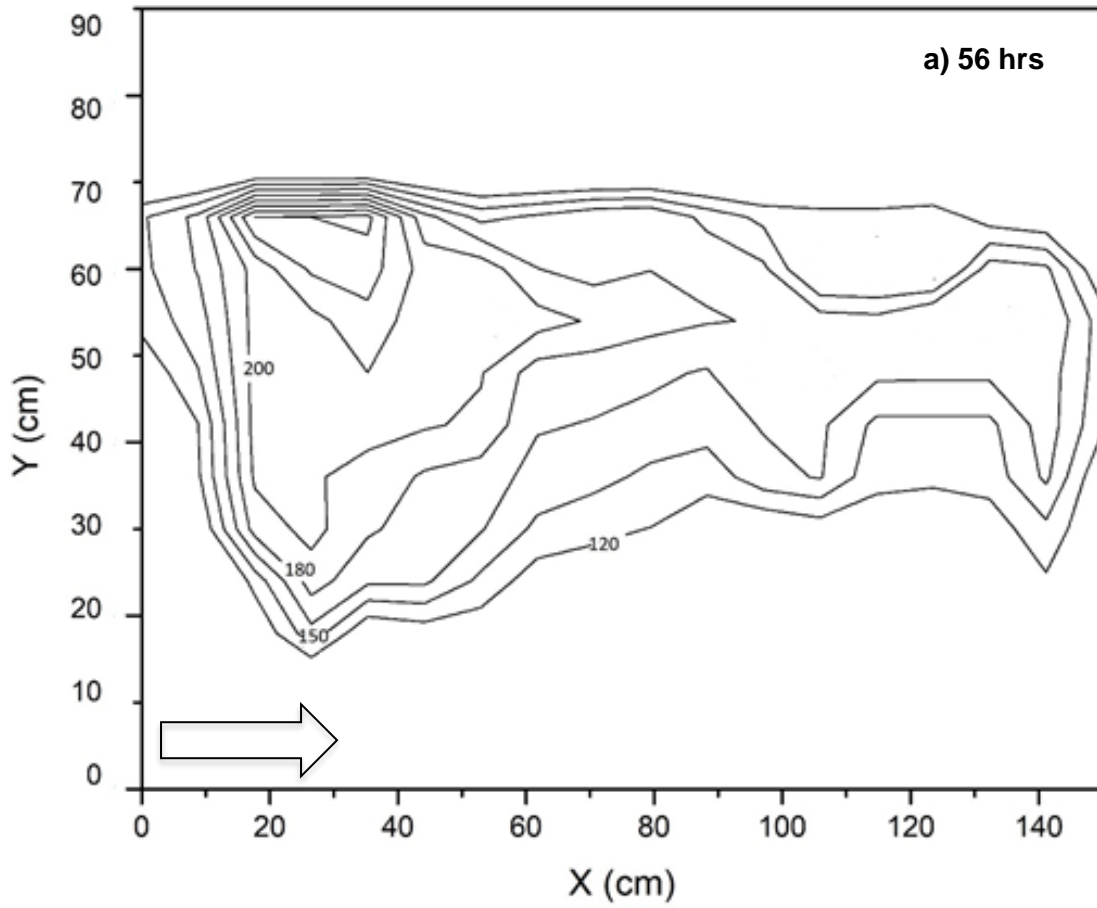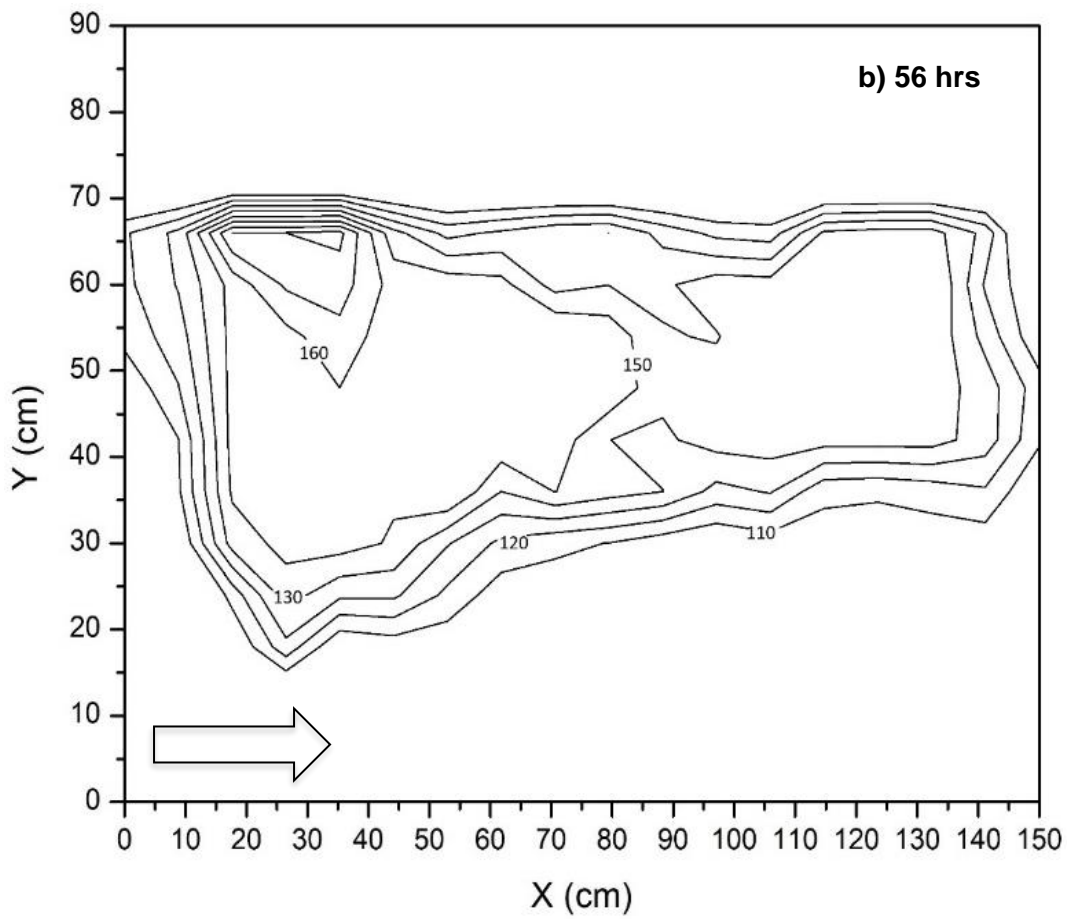491 stable groundwater regimes.

492

493

494

c) 24 hrs

495

d) 24 hrs

496

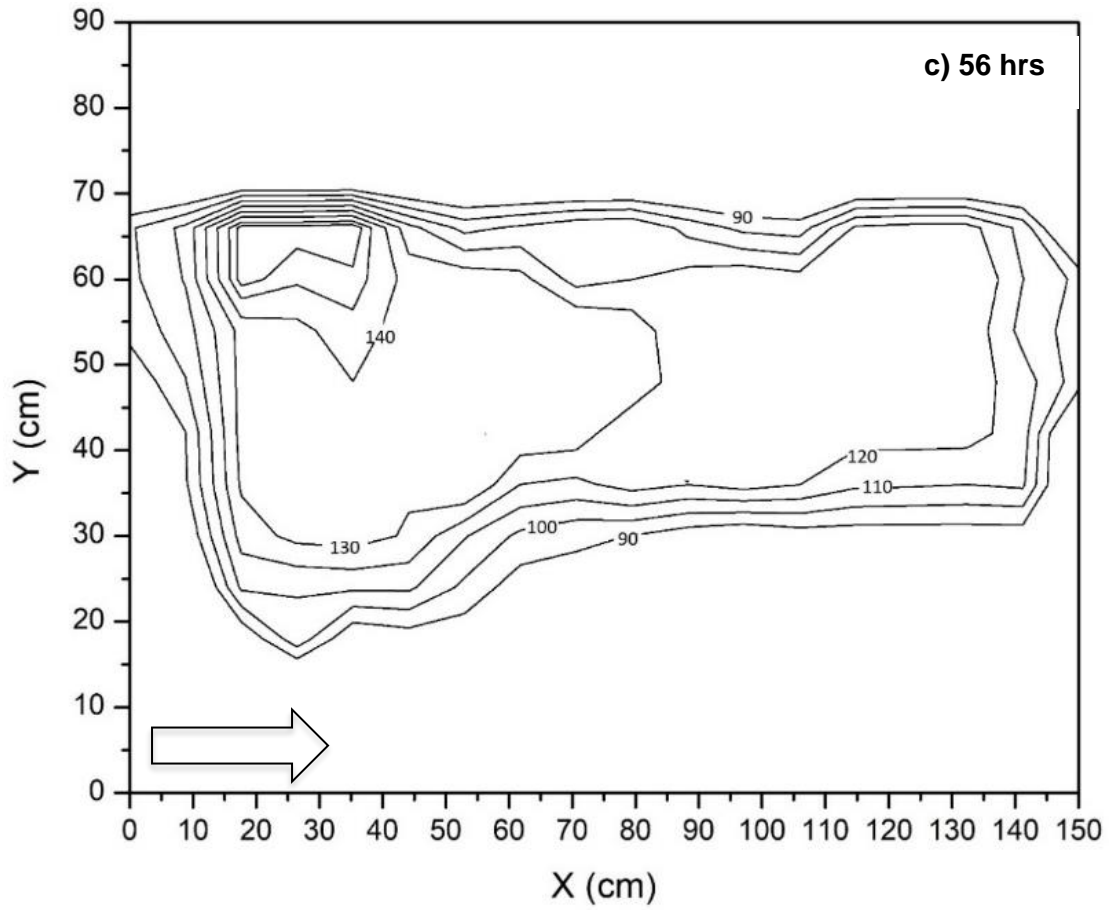a) 56 hrs
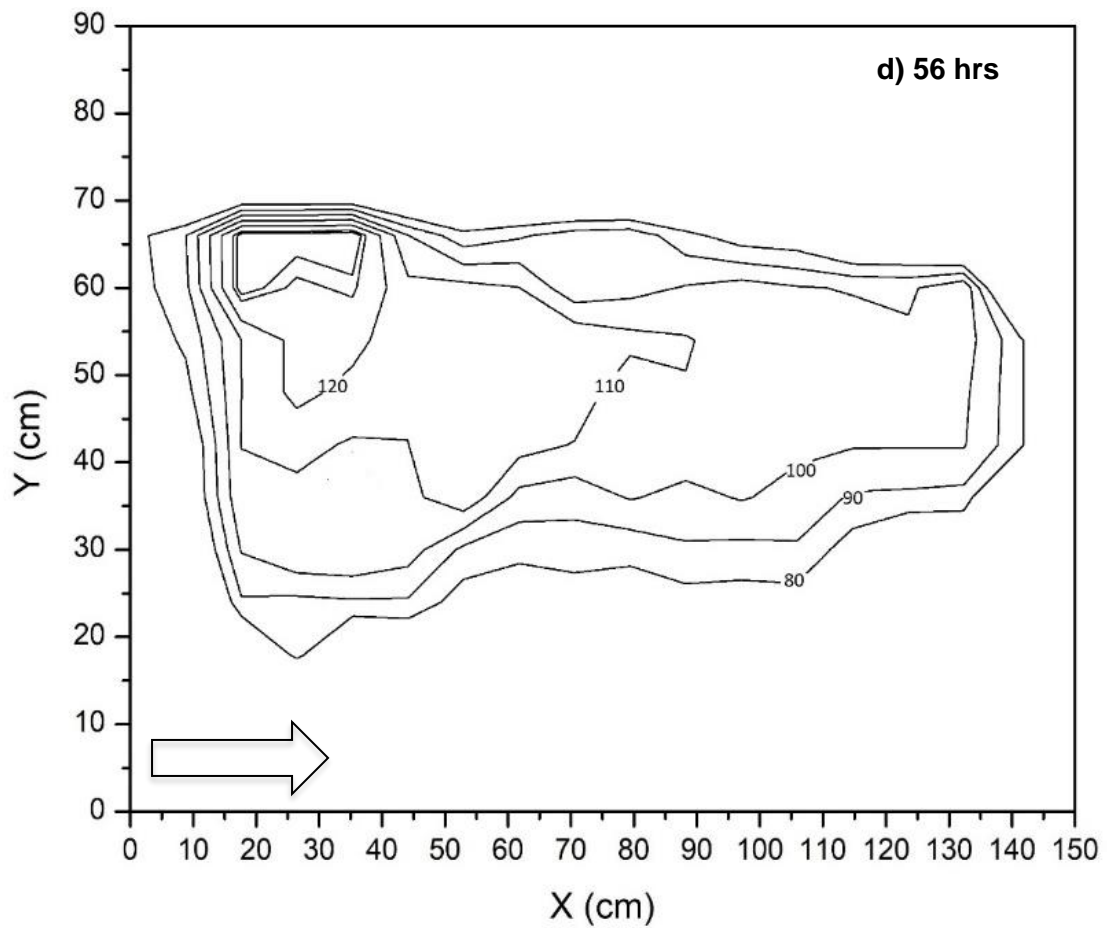
497

b) 56 hrs

498

c) 56 hrs

499

d) 56 hrs
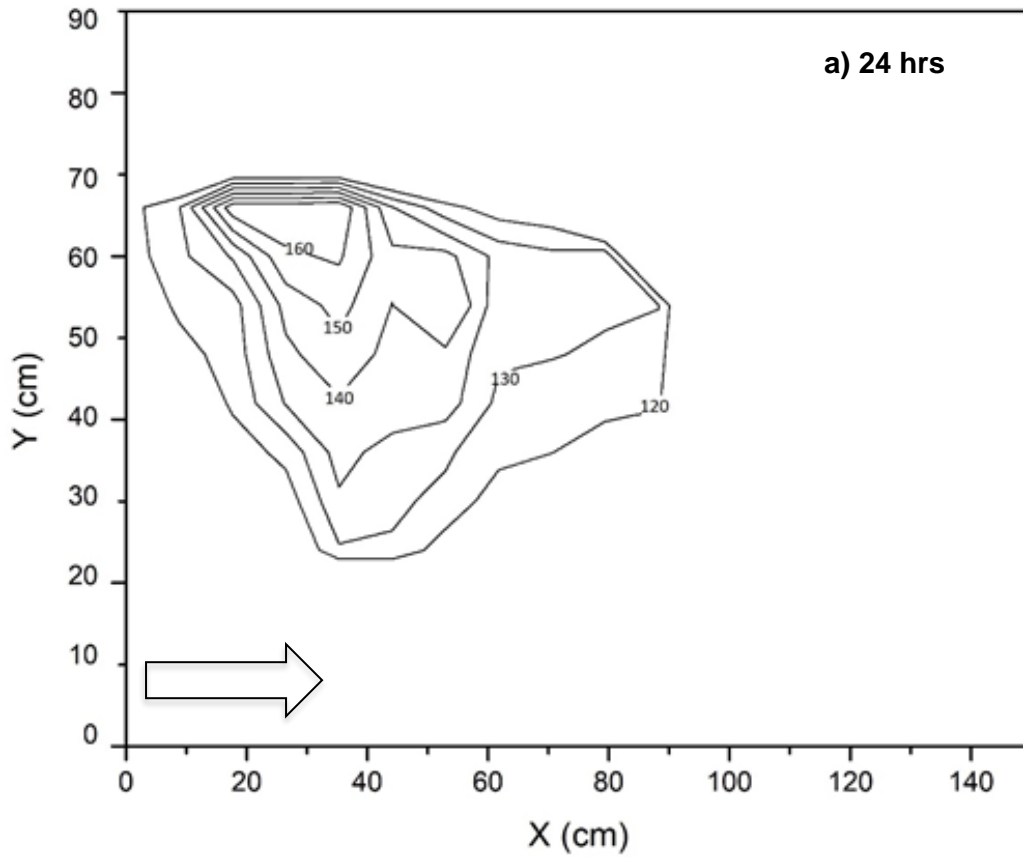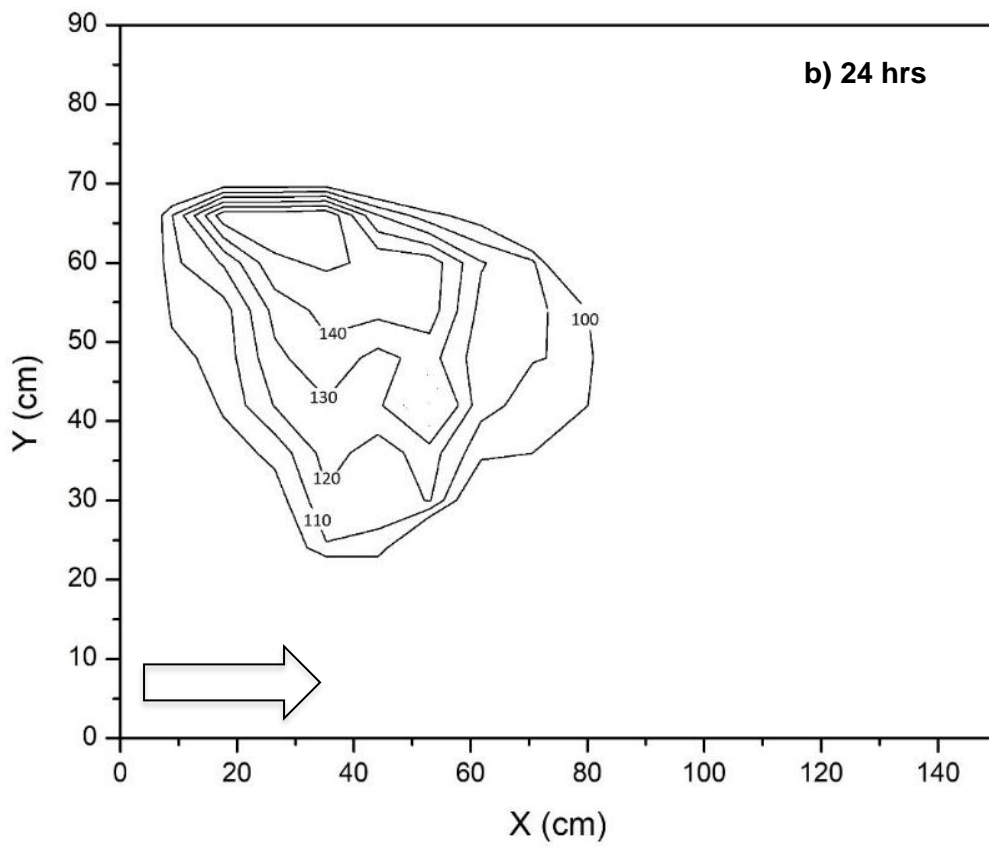
500

501   Figure 8: Concentration isolines presenting the extension of dissolved LNAPL plume

502   originated from pure phase source under a) rapid, b) general, c) slow and d) stable

503   groundwater table fluctuation cases.

504

505   4.4 Biodegradation under different groundwater table fluctuation conditions

506   Biodegradation rate of dissolved LNAPL plume originated from pooled LNAPL under stable

507   and fluctuating groundwater conditions was also investigated. For this purpose, spatial

508   biodegradation rates were estimated for port 1 and port 4 of upper sampling layer and port 8

509   and 14 of lower sampling layer. In Figure 9, the biodegradation rates were estimated using

510   corresponding values of equilibrium concentration of upward port and subsequent downward

511   port. Figure 9a presents biodegradation rate of port 4 situated 55 cm away from LNAPL pool.

512   At this location, biodegradation rates of 0.5 ppm/hour, 0.55 ppm/hour, 0.26 ppm/hour, and 0.13

513   ppm/hour were observed for dissolved LNAPL zone with the concentration of 180 ppm, 150

514   ppm, 120 ppm, and 100 ppm under rapid, general, slow and stable groundwater table condition,

515   respectively.

516   The biodegradation rate was found comparatively low in case of rapid fluctuation than general

517   fluctuation because of large high concentration (>150 ppm) region which causes toxic effects

518   on potential microbes lies in this region. While, the high biodegradation rate in case of general

519   than slow and stable groundwater fluctuation conditions proves the dependency of microbes

520   on dissolved LNAPL concentrations. Figure 9b represents biodegradation rates for port 7 of

521   upper layer having dissolved LNAPL concentration in the range of 100 ppm-150 ppm.

522   Similarly, Figure 9c and 9d shows the biodegradation rates for port 8 and port 14 of lower layer

523   respectively. Comparatively low biodegradation rates were observed in lower layer ports under

524   stable groundwater conditions, even if the dissolved LNAPL concentration was in the optimum

525   range of 100 ppm-150 ppm. These low biodegradation rate at lower ports was due to

526   comparatively less populated potential microbes due to low oxygen level. While, the

527   biodegradation rates were also increases at lower port in case of fluctuating groundwater

528   conditions. These accelerated biodegradation rate can attribute to the fact that the additional

529   oxygen to background level was added due to fluctuation in water table, which enhance the

530   microbial growth.

531   Microbial population was also counted using standard plate count method for periodically

532   collected soil-water samples from port 1 and port 7 of upper layer and port 8 and port 14 of

533   lower layer. The estimated CFU of collected soil-water samples were listed in table 4.

534   Initially, microbial count of 216.2-258 $\times 10^4$ CFU/mL and 142.5-147.2 $\times 10^4$ CFU/mL was

observed at upper and lower layer respectively. In GWTF-C1 case, the microbial count at port 1 increases upto 305×10^4 CFU/mL in 24 hours and then decreases to 78×10^4 CFU/mL in 56 hours. Similarly, at port 7, overgrowth was recorded after 24 hours thereafter decreases to 224×10^4 CFU/mL in 56 hours.

The enhanced microbial growth was observed as dissolved LNAPL concentration reached around 140-150 ppm at this location which provides sufficient carbon source to microbes. However, when the dissolved LNAPL concentration reaches higher than 150 ppm, it become toxic to microbial community. Increasing microbial count was recorded at both port of top layer due to optimum dissolved LNAPL concentration and sufficient oxygen level in general and slow groundwater fluctuation. Microbial count was recorded very low at port 14 of lower layer due to low concentration of dissolved LNAPL and insufficient oxygen level under all groundwater table conditions. Growing population of the microbial community at petroleum hydrocarbon-contaminated groundwater observed due to seasonal groundwater level fluctuations by Zhou et al. (2015). Such microbial analysis may help to implement nutrient and or electron acceptor plan to enhance petrochemical degrading microbes.
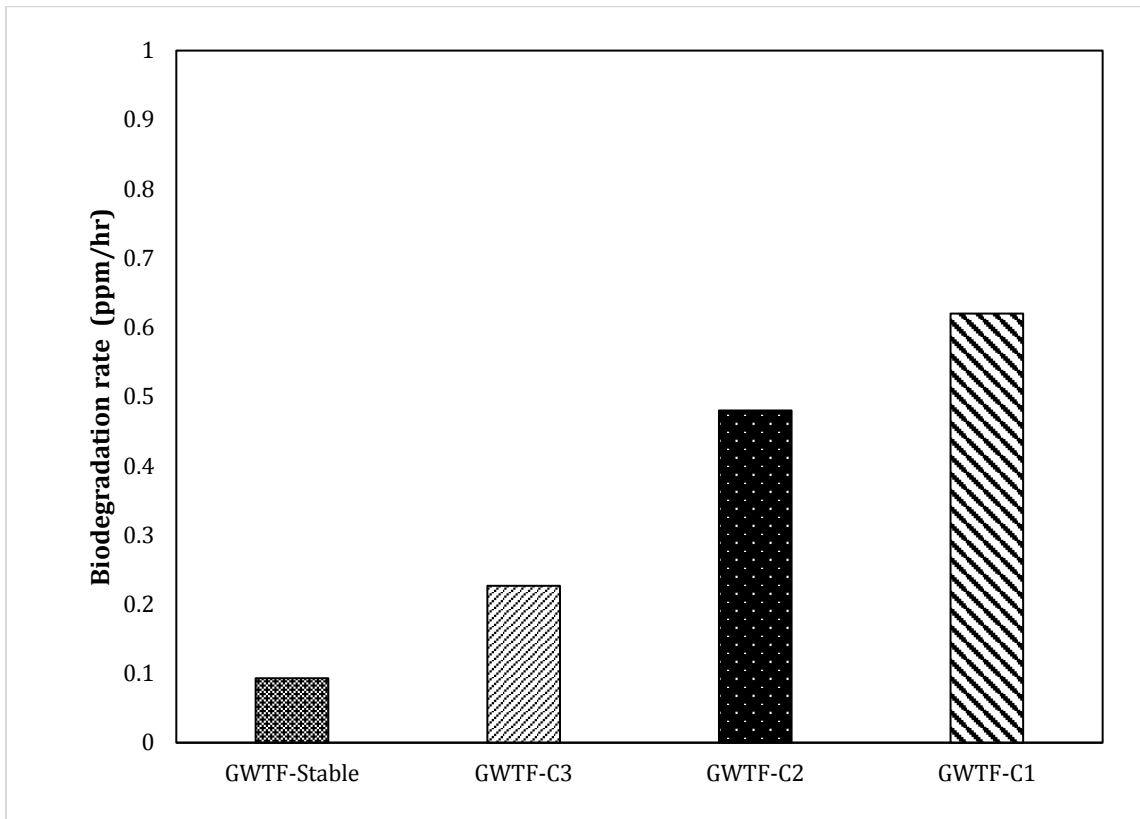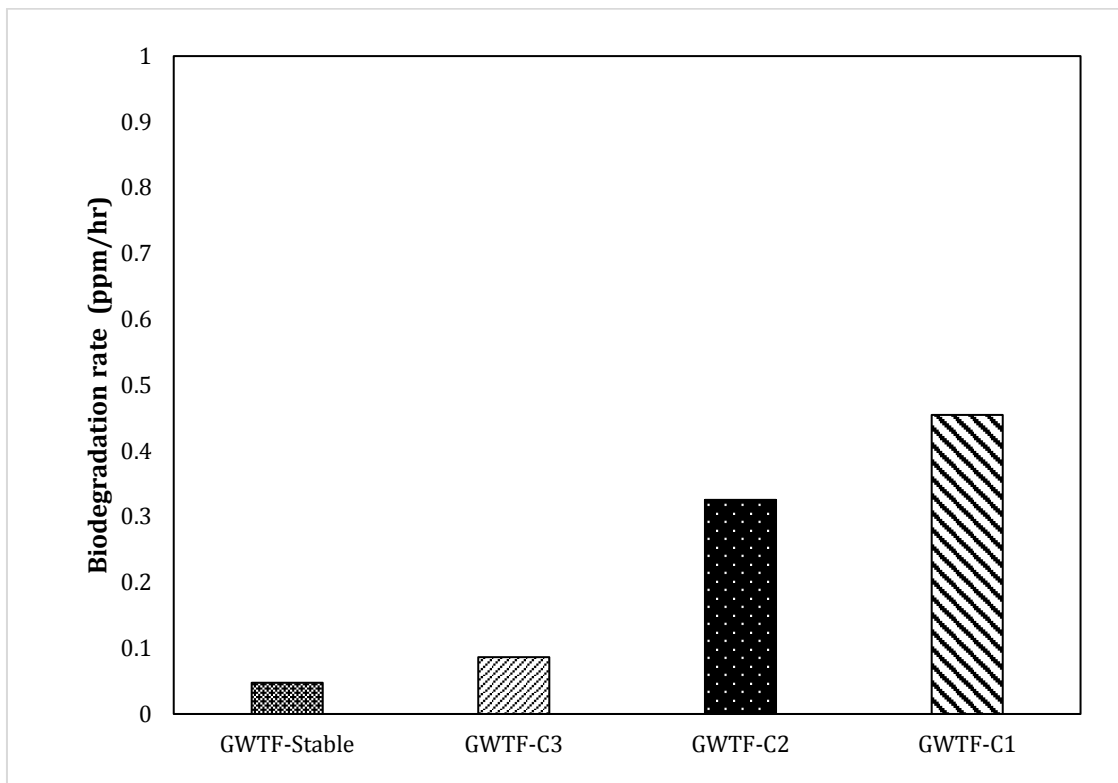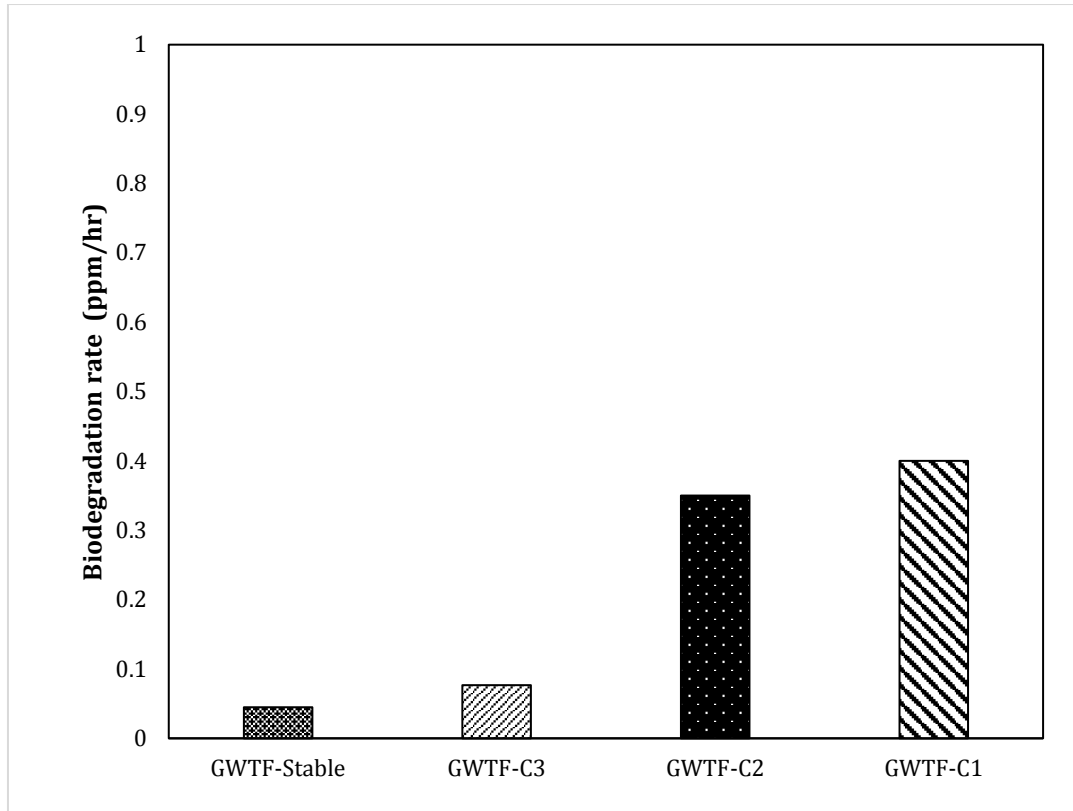

(a)

554

(b)

(c)

555

556

557

558

559

(d)
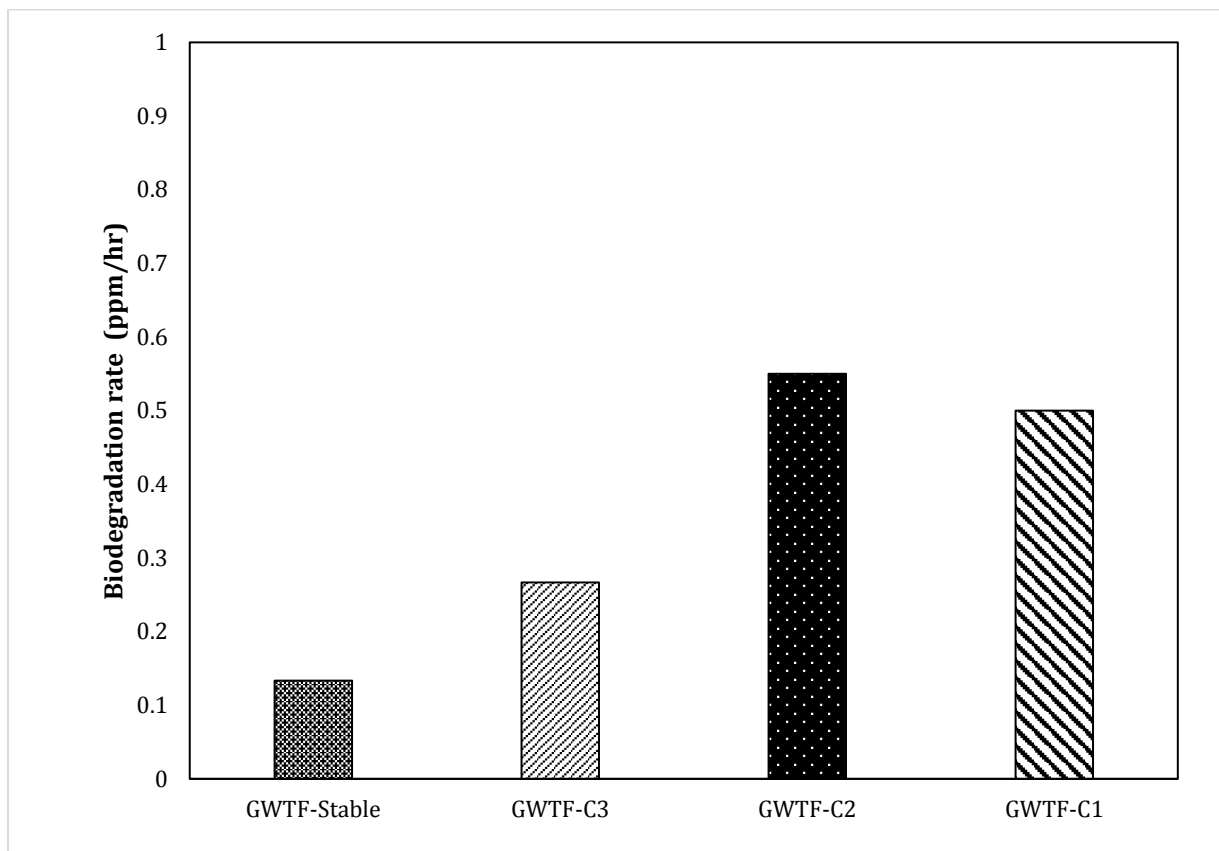
Figure 9: Biodegradation rates under stable and fluctuating groundwater conditions observed at (a) port 1 and (b) port 7 of upper sampling layer and (c) port 8 and (d) port 14 of bottom sampling layer of 2D sand tank setup.

Table 4. Microbial population count of samples collected from the experimental setup under different groundwater table conditions.

Condition	Port 1			Port 7			Port 8			Port 14		
	10^4 CFU/mL			10^4 CFU/mL			10^4 CFU/mL			10^4 CFU/mL		
	0hr	24hr	48hr	0hr	24hr	48hr	0hr	24hr	48hr	0hr	24hr	48hr
GWFT-C1	254.5	305	78	258.0	O	224.5	147.2	165	135.4	142.5	145.8	165
GWFT-C2	232.1	294.8	304.6	-	285.0	O	145	174.2	235.0	-	164.5	218
GWTF-C3	216.2	285.4	277.5	224.5	288.0	O	144.5	210.5	270.6	-	164.2	235.6

O= Overgrowth

574 **5. Conclusion**

575 In this study, a series of laboratory experiments and numerical modelling was performed to

576 investigate fate and transport of LNAPL originated from pure phase LNAPL pool under stable

577 and fluctuating groundwater conditions. Three different groundwater fluctuating

578 experiments representing rapid, general and slow groundwater table fluctuation scenarios

579 were conducted by raising/falling water table by 5cm of magnitude in 1, 2, and 4 hours

580 respectively. Estimated pool area shows a large pure phase LNAPL pool in smear zone

581 under fluctuating groundwater conditions, resulting in accelerating dissolution rate from

582 large LNAPL-water interphase area. Simulated and observed BTCs show high dissolved

583 LNAPL concentration and large plume originated from large LNAPL-water interphase area

584 under rapid groundwater fluctuation condition. The time of arrival of plume shows that

585 transport of dissolved LNAPL was comparatively more in case of rapid fluctuating

586 groundwater condition. A high biodegradation rate was observed in regions having

587 concentration ranges from 140-160 ppm of dissolved LNAPL. While, low biodegradation rates

588 were observed for low dissolved LNAPL concentrations (<140 ppm) and also high

589 concentrations (>160ppm) which fortifies the dependency on initial dissolved LNAPL

590 concentrations. Further, microbial growth was found to be increasing as plume moves away

591 from the LNAPL pool, which shows detrimental impact of high concentration of toluene on

592 survival of indigenous microorganisms. Overall, this study suggest that groundwater table

593 fluctuations significantly affects the distribution, transport, and biodegradation of the LNAPL

594 contaminants in subsurface. The results of this study may be improved by considering

595 subsurface heterogeneity and fractures. This study may help in design, establishment and

596 implementation of bioremediation techniques to decontaminate LNAPL polluted sites,

597 especially under varying subsurface conditions.

598

604

605 **References**

606   Basu, S., Yadav, B. K., and Mathur, S. 2015. Enhanced bioremediation of BTEX contaminated
607   groundwater in pot-scale wetlands. Environmental science and pollution Research.
608   22(24), 20041-20049.

609   Brusseau, M. L., Zhang, Z., Nelson, N. T., Cain, R. B., Tick, G. R., and Oostrom, M. 2002.
610   Dissolution of non-uniformly distributed immiscible liquid: intermediate-scale
611   experiments and mathematical modeling. Environmental science and technology. 36(5),
612   1033-1041.

613   Cherry J.A; Parker B.L; Bradbury K.R; Eaton T.T; Gotkowitz M.G; Hart; Borchardt M.A.,
614   2004. Role of Aquitards in the Protection of Aquifers from Contamination: A "State of
615   the Science" Report, Published by the Awwa Research Foundation, Denver, CO 80235-
616   3098.

617   Chrysikopoulos, C.V., 1995. Three-dimensional analytical models of contaminant transport
618   from nonaqueous phase liquid pool dissolution in saturated subsurface formations. Water
619   resource research. 31, 1137–1145.

620   Chrysikopoulos, C.V., Voudrias, E.A., Fyrillas, M.M., 1994. Modeling of contaminant
621   transport resulting from dissolution of nonaqueous phase liquid pools in saturated porous
622   media. Transport in Porous Media 16, 125–145.

623   Das, D. B. 2002. Hydrodynamic modelling for groundwater flow through permeable reactive
624   barriers. Hydrological Processes, *16*(17), 3393-3418.

625   Das, D. B., and Mirzaei, M. 2012. Dynamic effects in capillary pressure relationships for two-
626   phase flow in porous media: Experiments and numerical analyses. AIChE
627   Journal, *58*(12), 3891-3903.

628   Das, D. B., and Nassehi, V. 2003. Modeling of contaminants mobility in underground domains
629   with multiple free/porous interfaces. Water Resources Research, *39*(3).

630   Dempster, H.S., Sherwood-Lollar, B., Feenstra, S., 1997. Tracing organic contaminants in
631   groundwater: a new methodology using compound-specific isotopic analysis.
632   Environmental science and technology. 31, 3193–3197.

633   Dobson, R., M.H. Schroth, and J. Zeyer. 2007. Effect of water-table fluctuation on dissolution
634   on and biodegradation of a multi-component, light nonaqueous-phase liquid. Journal of
635   contaminant hydrology. 94, 235–248.

636   Herzyk, A., Fillinger, L., Larentis, M., Qiu, S., Maloszewski, P., Hünniger, M., Schmidt, S.I.,
637   Stumpp, C., Marozava, S., Knappett, P.S. and Elsner, M., 2017. Response and recovery

638   of a pristine groundwater ecosystem impacted by toluene contamination–A meso-scale
639   indoor aquifer experiment. Journal of contaminant hydrology. 207, 17-30.

640   Illangasekare, T.H., E. J. Armbruster, D. N. Yates, 1995. Non-aqueous-phase fluids in
641   heterogeneous aquifers - Experimental study. Journal of environmental engineering. 121,
642   571-579.

643   Kamaruddin SA, Sulaiman WNA, Rahman NA, Zakaria MP, Mustaffar M, Sa'ari R., 2011. A
644   review of laboratory and numerical simulations of hydrocarbons migration in subsurface
645   environments. Journal of environmental science and technology. 4(3), 191–214.
646   doi:10.3923/jest.2011.191.214.

647   Kechavarzi C., Soga K., Illangasekare T. H., 2005. Two-dimensional laboratory simulation of
648   LNAPL infiltration and redistribution in the Vadose zone. Journal contaminant
649   hydrology. 76(3–4):211–233.

650   Kim, T. J., and C. V. Chrysikopoulos, 1999. Mass transfer correlations for nonaqueous phase
651   liquid pool dissolution in saturated porous media, Water resource research. 35(2), 449–
652   459.

653   Kumar, A., Datta, M., Nema, A. K., and Singh, R. K. 2016. An improved rating system for
654   assessing surface water contamination potential from MSW landfills. Environmental
655   Modeling and Assessment, 21(4), 489-505.

656   Lee, K. Y., and C. V. Chrysikopoulos, 1998. NAPL pool dissolution in stratified and
657   anisotropic porous formations, J. Environmental engineering. 124(9), 851–862.

658   Legout C, Molenat J, Hamon Y., 2009. Experimental and modeling investigation of unsaturated
659   solute transport with water-table fluctuation. Vadose zone journal. 8:21–31.

660   Lenhard R. J., Oostrom M, Dane J.H., 2004. A constitutive model for air- NAPL-water flow in
661   the vadose zone accounting for immobile, non-occluded (residual) NAPL in strongly
662   water-wet porous media. Journal contaminant hydrology. 71(1–4):261–282.

663   Mobile, M. A., Widdowson, M. A., and Gallagher, D. L. 2012. Multicomponent NAPL source
664   dissolution: Evaluation of mass-transfer coefficients. Environmental science and
665   technology. 46(18), 10047-10054.

666   Mustapha, H. I., Gupta, P. K., Yadav, B. K., van Bruggen, J. J. A., and Lens, P. N. L. 2018.
667   Performance evaluation of duplex constructed wetlands for the treatment of diesel
668   contaminated wastewater. Chemosphere, *205*, 166-177.

669 Nambi, I.M., and Powers, S.E., 2000. NAPL dissolution in heterogeneous systems: an
670   experimental investigation in a simple heterogeneous system. Journal contaminant
671   hydrology. 44, 161–184.

672 Nambi, I.M., and Powers, S.E., 2003. Mass transfer correlations for nonaqueous phase liquid
673   dissolution from regions with high initial saturations. Water resource research. 39 (2).

674 Neale, C. N., Hughes, J. B., and Ward, C. H., 2000. Impacts of unsaturated zone properties on
675   oxygen transport and aquifer reaeration. Groundwater. 38(5), 784-794.

676 Nema, A. K., and Gupta, S. K. 1999. Optimization of regional hazardous waste management
677   systems: an improved formulation. Waste Management, *19*(7-8), 441-451.

678 Nema, A. K., and Gupta, S. K. 2003. Multiobjective risk analysis and optimization of regional
679   hazardous waste management system. Practice Periodical of Hazardous, Toxic, and
680   Radioactive Waste Management, *7*(2), 69-77.

681 Oostrom, M., Dane, J. H., and Wietsma, T. W., 2007. A review of multidimensional, multifluid,
682   intermediate-scale experiments: Flow behavior, saturation imaging, and tracer detection
683   and quantification. Vadose zone journal. 6(3), 610-637.

684 Oostrom, M., Hofstee, C., and Wietsma, T. W. 2006. LNAPLs do not always float: an example
685   case of a viscous LNAPL under variable water table conditions (No. PNNL-SA-48870).
686   Pacific Northwest National Laboratory (PNNL), Richland, WA (US), Environmental
687   Molecular Sciences Laboratory (EMSL).

688 Patterson B. M. and Davis G. B., 2009. Quantification of vapor intrusion pathways into a slab-
689   on-ground building under varying environ- mental conditions. Environ Science and
690   Technology. 43(3):650–656.

691 Picone, S., Grotenhuis, T., van Gaans, P., Valstar, J., Langenhoff, A., and Rijnaarts, H., 2013.
692   Toluene biodegradation rates in unsaturated soil systems versus liquid batches and their
693   relevance to field conditions. Applied microbiology and biotechnology. 97(17), 7887-
694   7898.

695 Power S.E. and Heermann S.E., 1999. Potential ground and surface water impacts, appendix
696   B: Modeling interface mass-transfer processes" presented in "A critical review: the effect
697   of ethanol in gasoline on the fate and transport of BTEX in the subsurface", Editors
698   Cannon G. and Rice D., UCRL-AR-135949 Vol.4, chapter 2.

699   Powers, S.E., Abriola, L.M., Dunkin, J.S., Weber, W.J., 1994a. Phenomenological model for
700   transient NAPL–water mass transfer processes. Journal contaminant hydrology. 16, 1–
701   33.

702   Powers, S.E., Abriola, L.M., Weber Jr., W.J., 1992a. An experimental investigation of
703   nonaqueous phase liquid dissolution in saturated subsurface systems: steady state mass
704   transfer rates. Water resource research. 28 (10), 2691 – 2705.

705   Powers, S.E., Abriola, L.M., Weber, W., 1994b. An experimental investigation of NAPL
706   dissolution in saturated subsurface systems: transient mass transfer rates. Water resource
707   research. 30, 321–332.

708   Powers, S.E., Abriola, L.M., Weber, W.J., 1992b. An experimental investigation of
709   nonaqueous phase liquid dissolution in saturated subsurface systems: steady state mass
710   transfer rates. Water resource research. 28 (10), 2691–2705.

711   Rivett, M.O., Wealthall, G.P., Dearden, R.A., McAlary, T.A., 2011. Review of unsaturated-
712   zone transport and attenuation of volatile organic compound (VOC) plumes leached from
713   shallow source zones. Journal of contaminant hydrology 123, 130-156.

714   Rolle, M., Eberhardt, C., Chiogna, G., Cirpka, O. A., and Grathwohl, P., 2009. Enhancement
715   of dilution and transverse reactive mixing in porous media: Experiments and model-
716   based interpretation. Journal of contaminant hydrology, 110(3-4), 130-142.

717   Saba, T.A., Illangasekare, T.H., 2000. Effect of ground-water flow dimensionality on mass
718   transfer from entrapped nonaqueous phase liquid contaminants. Water resource research.
719   36 (4), 971 – 979.

720   Sarikurt, D. A., Gokdemir, C., and Copty, N. K., 2017. Sherwood correlation for dissolution of
721   pooled NAPL in porous media. Journal of contaminant hydrology. 206, 67-74.

722   Simunek, J., T. Vogel, and M.Th. van Genuchten., 1996. HYDRUS-2D code for simulating
723   water flow and solute transport in two-dimensional variably saturated media. Version
724   1.0. USDA/ARS, U.S. Salinity Lab., Riverside, CA.

725   Šimunek, J., Van Genuchten, M. T., and Šejna, M. (2012). HYDRUS: Model use, calibration,
726   and validation. Transactions of the ASABE, 55(4), 1263-1274.

727   Sulaymon, A., and H.A. Gzar., 2011. Experimental investigation and numerical modelling of
728   light non-aqueous phase liquid dissolution and transport in a saturated zone of the soil.
729   Journal of Hazardous Materials. (186), 1601–1614.

730   Vasudevan, M., G. Suresh Kumar, N. Indumathi M., 2014. Numerical study on
731   kinetic/equilibrium behaviour of dissolution of toluene under variable subsurface
732   conditions. European journal of environmental and civil Engineering. 18(9), pp.1070–
733   1093.

734   Yadav B.K., and Hassanizadeh S.M., 2011. An overview of biodegradation of LNAPLs in
735   coastal (semi)-arid environment. Water air soil pollution. 220, 225-239.

736   Yadav B.K., Ansari FA, Basu S, Mathur A., 2013. Remediation of LNAPL contaminated
737   groundwater using plant-assisted biostimulation and bioaugmentation Methods". Water
738   air soil pollution. 225, 1793.

739   Yadav, B.K., Shrestha, S.R. and Hassanizadeh, S.M., 2012. Biodegradation of toluene under
740   seasonal and diurnal fluctuations of soil-water temperature. Water, air, and soil pollution,
741   223(7), pp.3579–3588.

742   Zhang Q, Wang G.C., Sugiura N, Utsumi M, Zhang ZY, Yang YN., 2014. Distribution of
743   petroleum hydrocarbons in soils and the underlying unsaturated subsurface at an
744   abandoned petrochemical site, North China. Hydrological process. 28, 2185–2191.

745   Zhou, A. X., Zhang, Y. L., Dong, T. Z., Lin, X. Y., and Su, X. S., 2015. Response of the
746   microbial community to seasonal groundwater level fluctuations in petroleum
747   hydrocarbon-contaminated groundwater. Environmental science and pollution
748   research. 22(13), 10094-10106.

Assessment of LNAPL in subsurface under fluctuating groundwater table using 2D sand tank experiments

Gupta, Pankaj Kumar